3

Numerical Methods in Micromechanical Contact

Vladislav A. YASTREBOV
CNRS, Mines Paris PSL, France

3.1. Introduction

Mechanical contact and all associated mechanisms such as friction, wear, adhesion and mixed lubrication regimes represent critical mechanisms in many natural (such as small animal legs, joints, glaciers and faults) and industrial systems (tires/pavement, gears, bearings and piston/cylinder, for example). Very often, in the analysis of these systems, it is assumed that contact surfaces have nominal shapes smooth almost everywhere. However, in reality, all real surfaces, especially those found in nature, exhibit much more complex shapes than their nominal forms: in other words, we can say that these surfaces are rough. This roughness influences almost all interfacing phenomena (Bowden and Tabor 1986; Vakis et al. 2018): the stress state near the contact, the contact interface stiffness, wear, friction, adhesion, heat and electrical transfer as well as watertightness are all affected by the roughness of the surfaces in contact. In most cases, at the macroscopic scale (the scale of the nominal contact area and structure), the effect of roughness can be taken into account by phenomenological laws or those based on microscopic considerations (Greenwood 1966; Cooper et al. 1969; Zavarise et al. 1992), including Archard's law of wear (Archard and Hirst 1956), Coulomb's law of friction as well as other laws

For a color version of all figures in this chapter, see www.iste.co.uk/lebon/mechanics.zip.

Numerical Methods for Strong Nonlinearities in Mechanics,
coordinated by Jacques BESSON, Frédéric LEBON and Eric LORENTZ.

such as "rate and state" friction (Rice and Tse 1986; Dieterich 1992; Dieterich and Kilgore 1994; Rice 2006). However, micromechanical models used in the past were based on fairly simplistic roughness and mechanical behavior models. Often, these limitations came from the need to make strong enough assumptions to obtain results because the contact problem formulated for complex geometry cannot be solved analytically due to its high nonlinearity. Now, considering advanced numerical methods and today's computing power, a large field of applications in micromechanical contact is becoming highly accessible to researchers and engineers. This chapter discusses advances in numerical methods and our increasing understanding of small-scale contact physics.

3.1.1. *Plan*

This chapter is organized as follows. First, the contact problem and its micromechanical nature are presented in section 3.2. The finite element method (FEM) is briefly discussed in section 3.3 with emphasis on features relevant to small-scale contact. The boundary element method is not presented in detail in this chapter, so an interested reader should refer to a recent review by Bemporad and Paggi (2015). Nevertheless, many applications of this method to small-scale contact problems are presented. Two main applications of micromechanical contact: the contact between rough edges and contact between rough surfaces are covered in sections 3.4 and 3.5, respectively. Some problems for the future are formulated in section 3.6.

3.2. Contact micromechanical problem

3.2.1. *Surface geometry: mathematical description*

In this section, we formulate the micromechanical problem of contact. This will form the subject of the following sections. We consider the contact between two simply related bodies[1] (open sets $\Omega^1(t), \Omega^2(t)$) with one or more surfaces exhibiting "roughness"[2]. The configuration is defined at each time t, in the following this explicit notation of this time dependency will be omitted. The mechanical behavior of materials (homogeneous or heterogeneous) can be linear or nonlinear, while the contact model can be considered without or with friction/adhesion. In the general case, in the initial state, the two potential contact surfaces are described by vectors:

1 The simple connectedness condition of bodies in contact makes it possible to somewhat simplify the mathematical formulation, especially in terms of the application of parametric space in physical space.

2 "Roughness" refers here to any surface shape.

$$\begin{cases} \boldsymbol{r}^1(\xi^1,\eta^1) \in \partial\Omega^1 \\ \boldsymbol{r}^2(\xi^2,\eta^2) \in \partial\Omega^2 \end{cases} \quad \boldsymbol{r}^1, \boldsymbol{r}^2 \in \mathbb{R}^3$$

where $\partial\Omega^i$ defines the closure of the set, $\boldsymbol{r}^1, \boldsymbol{r}^2$ are at least surjective mappings[3] of parameters $\{\xi^i, \eta^i\} \in \mathcal{X}^i \subset \mathbb{R}^2$, $i = 1, 2$ in two-surfaces $\partial\Omega^i$ emerged in the three-dimensional physical space $\mathbb{R}^3$:

$$\boldsymbol{r}^i : \mathcal{X}^i \subset \mathbb{R}^2 \to \partial\Omega^i \subset \mathbb{R}^3$$

The mapping $\boldsymbol{r}^i$ is continuous. Let us assume that $\mathcal{X}^i$ is simply connected and convex. Hereafter, we merely consider the problem of three-dimensional contact; the indexes $1, 2$ in superscript denote both surfaces. In principle, the formulation can be adapted to self-contact problems, where different parts of the same surface come into contact.

Contact can be achieved by way of different types of loading (mechanical, thermal, magnetic). This formulation of the contact problem is rather general and can be adapted to macroscopic and microscopic contact. However, we will consider that the geometry of both surfaces is very complex, unlike most macroscopic applications where the surfaces studied remain quite simple.

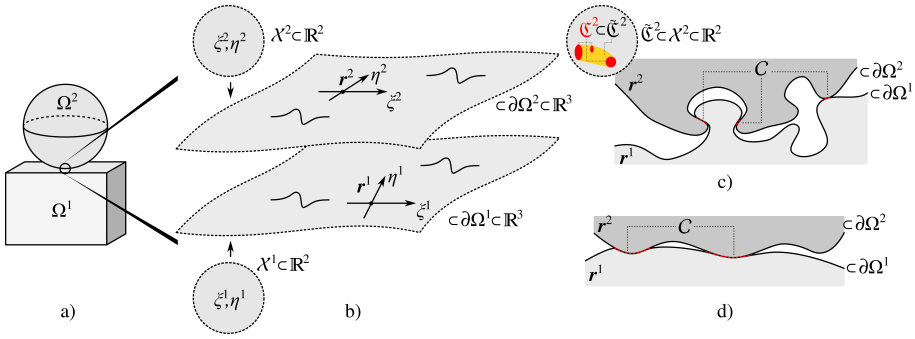

Figure 3.1. *Contact problem between two bodies on the surface: (a) the macroscopic scale; (b) magnification of surfaces parts potentially in contact (parameterization is indicated); (c) example of the non-simplifiable contact problem; (d) example of surfaces that allow an explicit representation at the given time*

Let us introduce the contact area $\mathcal{C}$ (with no self-contact) in the current configuration as a set of points $\boldsymbol{r}^c$ such that:

$$\mathcal{C} = \left\{ \boldsymbol{r}^c \in \mathbb{R}^3 \quad \middle| \quad \exists \boldsymbol{r}^1 \in \partial\Omega^1, \boldsymbol{r}^2 \in \partial\Omega^2 : \boldsymbol{r}^c = \boldsymbol{r}^1 = \boldsymbol{r}^2 \right\}$$

3 When there is no self-contact, these maps can be considered to be bijective.

Its images are denoted as:

$$\boldsymbol{r}^i : \mathfrak{C}^i \subset \mathcal{X} \rightarrow \mathcal{C} \subset \partial\Omega^i$$

Let the set $\tilde{\mathfrak{C}}^i \supset \mathfrak{C}^i$ also be introduced, such that $\tilde{\mathfrak{C}}^i$ is a simply connected and convex two-manifold of minimal size[4]. It should be noted that the sets $\mathfrak{C}$ and $\mathcal{C}$ are not necessarily connected sets, nor are they manifolds, and are not necessarily compact either. So that geometric quantities of different sizes can be compared, we define the linear size $T(\bullet)$ of an entity $\mathcal{A}$:

$$T(\mathcal{A}) = \max_{\boldsymbol{r},\boldsymbol{r}' \in \mathcal{A}} \|\boldsymbol{r} - \boldsymbol{r}'\|$$

where $\|\boldsymbol{a}\|$ defines a vector Euclidean norm. Let $\mathfrak{C}_0^i$ denote the maximal extension of the contact area in the parametric space $\mathfrak{C}_0^i \subset \mathcal{X}^i$, that is, $\forall t : \mathfrak{C}(t) \subseteq \mathfrak{C}_0^i \subseteq \mathcal{X}^i$. Naturally, $\mathfrak{C}_0^i$ is problem dependent and cannot always be guessed.

The surface has an *explicit form* in the area of interest. If at every time instant $t \in \mathcal{T}$ there exists an orthonormed basis $\boldsymbol{e}_x, \boldsymbol{e}_y, \boldsymbol{e}_z \in \mathbb{R}^3$, $\boldsymbol{e}_\alpha \cdot \boldsymbol{e}_\beta = \delta_{\alpha\beta}$, $\alpha, \beta \in \{x, y, z\}$ such that the surfaces in which the potential contact is located can be represented as functions $z^i(x, y)$, where $z^i = \boldsymbol{r}^i \cdot \boldsymbol{e}_z$, $x = \boldsymbol{r}^i \cdot \boldsymbol{e}_x$, $y = \boldsymbol{r}^i \cdot \boldsymbol{e}_y$:

$$\forall t \in \mathcal{T}, \exists \boldsymbol{e}_x, \boldsymbol{e}_y, \boldsymbol{e}_z \in \mathbb{R}^3 \text{ s.t. } \forall \boldsymbol{r}^i(\tilde{\mathfrak{C}}_0^i) : \exists!\ z^i(x, y) \text{ s.t. } \boldsymbol{r}^i = \boldsymbol{e}_z z^i(x, y) + \boldsymbol{e}_x x + \boldsymbol{e}_y y$$

where $\tilde{\mathfrak{C}}_0^i \supset \mathfrak{C}_0^i$ is, as introduced earlier, a simply connected and convex two-manifold of minimal size that includes $\mathfrak{C}_0^i$. More broadly, we will allow ourselves to work with surfaces that have a *semi-explicit* representation, which will be defined below. First, let the set $\mathbb{X} \in \mathbb{R}^2$ be defined such that it consists of all points: $\{\boldsymbol{r}^i(\tilde{\mathfrak{C}}_0^i) \cdot \boldsymbol{e}_x,\ \boldsymbol{r}^i(\tilde{\mathfrak{C}}_0^i) \cdot \boldsymbol{e}_y\}$. A semi-explicit surface is defined as a surface for which the set of points $\{x, y\} \in \mathbb{X}_n \subset \mathbb{X}$ for which $z^i(x, y)$ is not always unique and of zero measure. If the two surfaces do not have an explicit or semi-explicit shape as defined previously in the neighborhood of the potential contact area, the associated contact problem will be referred to as *unsimplifiable*. An example of a unsimplifiable problem is shown in Figure 3.1(c).

From this very general formulation, we could propose some particularly appealing sub-cases. When the linear dimension of the contact area is very small compared to the size of the bodies in contact $T(C) \ll T(\Omega_1), T(\Omega_2)$ and if we are

4 The convexity condition of $\mathcal{X}^i$ that was requested earlier comes from the need to ensure that: $\tilde{\mathfrak{C}}^i \subset \mathcal{X}^i$.

exclusively focusing on the state of strain and stress in the contact area, fields can be thought to be semi-infinite (see, for example, the theory of Hertz (1881)). If also, there is in the area of interest an existing explicit representation of the surfaces, and the maximum gradient is infinitesimal, that is, $\max|\nabla z(x,y)| \ll 1$, fundamental Boussinesq, Cerutti and Flamant solutions can be used. It is important to emphasize that these solutions are not usable when a deformable surface does not have an explicit representation in the vicinity of the contact zone.

3.2.2. *Surface geometry: examples and discussions*

"Roughness", or more generally the geometry, of natural and industrial surfaces, can take very varied forms. In Figure 3.2, some pictures of the various surfaces are assembled: (a) beach wrinkles formed by the interaction of sand particles with wind or current; (b) pebbles of different sizes; (c) the granite fracture surface; (d) the texture of a painted wall; (e) the creep fracture surface of a titanium superalloy; (f) "elephant skin" on rocks in the forest of Fontainebleau; (g) the surface of the sea; (h) the surface of a fibrous material; (i) peeling paint; (j) pebble pavement; (k) dry soil; (l) asphalt; (m) bark; (n) finger skin; (o) drops of water on car paint; and (p) the fracture surface (lower part) on a rock in the forest of Fontainebleau. The geometries presented here are all complex and show a random character. However, except for examples (c) and (g), the surface geometries in the pictures rather represents the mesoscopic scale which additionally contains a small-scale roughness, which will be discussed in a little more detail in section 3.2.3.

In addition, this geometry can be considered resolution dependent. This assertion is all the more true because at the atomic scale matter has no continuity, the latter is only a model. Nonetheless, this is a model that remains valid from the nanoscale and the one that will be employed in the context of this presentation. But even at the validity scales of the continuous medium model, surface geometry can be described at different levels of accuracy. Consider an example of a beach wrinkle (see Figure 3.2(a) where a "continuous" shape, which is nevertheless made up of sand particles which form at their scale a very complex "surface", similar to that of Figure 3.2(b) can be distinguished. In addition, the surface of the sand particles is also rough as in Figure 3.2(c). For this example, at least three scales can be distinguished: wrinkle, particles and roughness. Clearly, these three scales cannot be simultaneously treated in order to understand the interaction of the wheels of a rover on Mars with the ground of the Red Planet. Besides the difference in the scales of shape and roughness, there are many examples of surface geometries that distinguish different scales: turned surfaces, abrasion-polished surfaces and architected surfaces (Yoon et al. 2006; Autumn 2007; Costa and Hutchings 2007). We can note that although these scales are quite distinct at first glance, in some cases there is no separation between these scales in terms of mechanics (Greenwood and Tripp 1967; Yastrebov 2019).

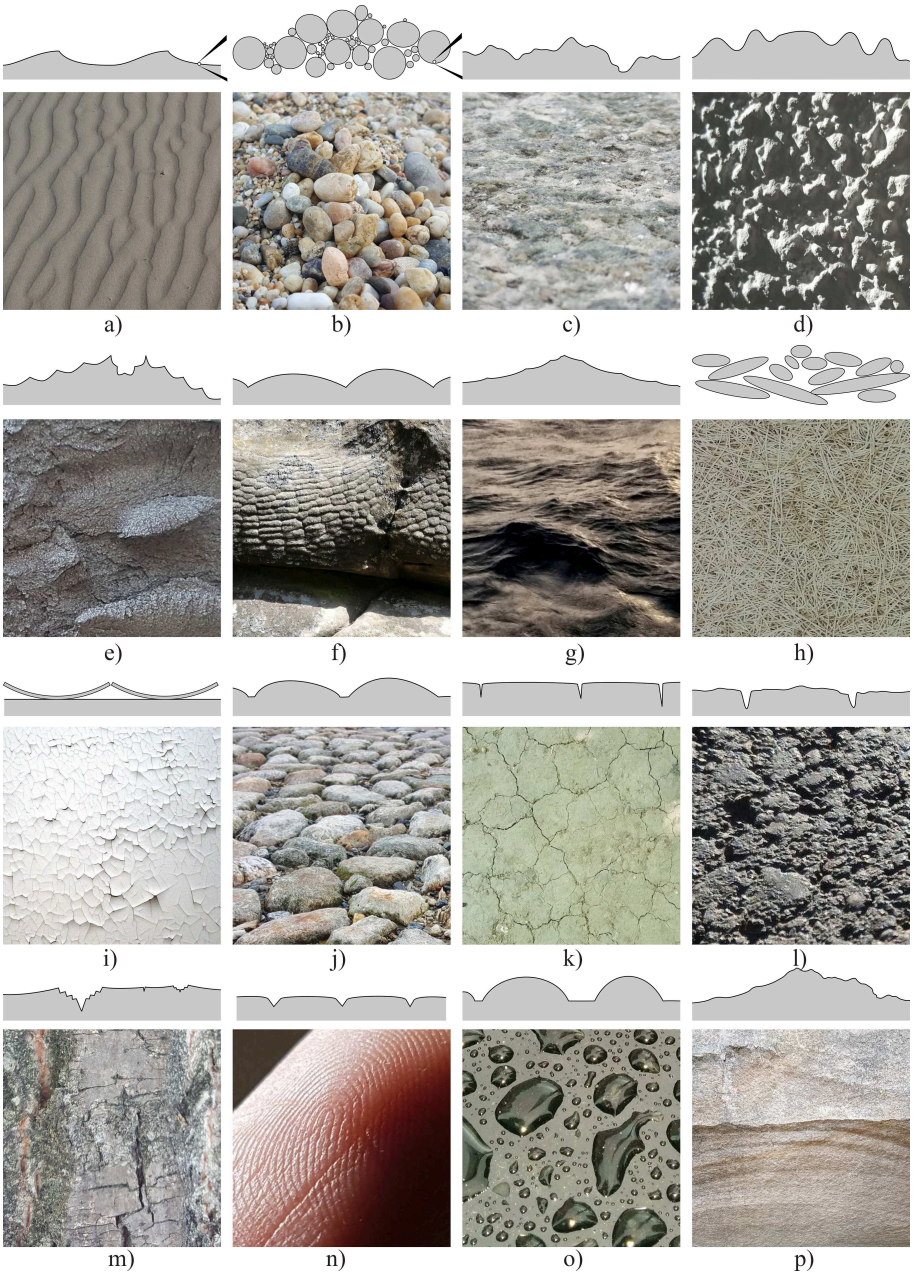

Figure 3.2. *Different geometries of natural surfaces*

Often, in contact problems, only the "shape" of the parts, as it was designed, is taken into consideration, but inevitably this shape hides aspects of the roughness that is the subject of this section. Form can often be defined as deterministic, especially in engineering applications while roughness is stochastic and random. However, it can also be addressed deterministically. Otherwise, the aspect of roughness can be taken into account by means of phenomenological relations that can be obtained, among other things, by deterministic calculations of the contact of rough surfaces or through statistical models.

3.2.3. *Roughness models*

The objective here is not to present in detail all aspects of rough surfaces; all of this information can be found in engineering (Thomas 1999; Whitehouse 2010), mathematical (Adler and Taylor 2009) or physics texts (Mandelbrot 1983; Meakin 1998). Nevertheless, it would be important to propose some references on modeling the geometry of rough surfaces. First, a model for a rough surface can be obtained by direct surface measurements, but since the resolution of all instruments is limited, the reconstruction of a final surface can be considered as modeling. In addition to direct measurements, different methods for modeling rough surfaces can be found. Often, these are methods that are based on a fractal characteristic of most natural and industrial surfaces (Russ 1994; Renard et al. 2013). A good review of these methods for addressing the mechanics of contact of rough surfaces was given in Zahouani et al. (1998). The simplest method is the *mid-point random displacement* (Russ 1994; Meakin 1998) which, in a hierarchical way, subdivides the grid of points at each iteration (a segment in two, a face in four) and in doing so, it disturbs the vertical coordinate of each new point in a random manner. To reach the fractal aspect, the standard deviation of these perturbations decreases with each new iteration. The rate of this decay depends on the fractal dimension of the modeled surface. On the other hand, the resulting surface requires smoothing (interpolation) in order to obtain a well-posed mechanical problem, that is, a problem for which mesh refinement leads to the convergence of the numerical solution. Another fairly common method makes use of the Weierstrass–Mandelbrot function generalized to problems with 2D surfaces by Majumdar and Tien (1990). This method does however not easily obtain isotropic surfaces (Zahouani et al. 1998). A powerful and flexible method is the spectral filtering method for white noise (Hu and Tonder 1992), which makes it possible to reproduce on average a self-affining spectrum with a defined Hurst exponent while presenting a certain level of stochasticity. In addition, this filtering can be used to introduce low- and high-frequency cuts, which results in obtaining smooth surfaces at the scale of discretization and the Gaussian distribution of heights (Yastrebov et al. 2015). Recently, a method for modeling surfaces with controlled height distribution was proposed in Pérez-Ràfols and Almqvist (2019).

3.2.4. *Contact formalization*

In this section, we will formalize contact conditions which can be summarized (with no friction and adhesion) by the following three conditions:

1) No penetration, that is, no intersection between solids $\Omega^1 \cap \Omega^2 = \emptyset$.

2) No adhesion $\boldsymbol{n} \cdot \boldsymbol{\sigma} \cdot \boldsymbol{n} \leq 0$, that is, the normal stress is not positive.

3) No shear at the contact interface, that is, the tangential component cancels out $(\boldsymbol{I} - \boldsymbol{n} \otimes \boldsymbol{n}) \cdot \boldsymbol{\sigma} = 0$, where $\boldsymbol{\sigma}$ is the Cauchy stress tensor, $\boldsymbol{n}$ is the outgoing normal and $\boldsymbol{I}$ is an identity tensor. Condition (1) can be reformulated as a kinematic inequality as follows: none of the points of a surface $\partial\Omega^1$ can penetrate the volume Ω^2, nor can penetrate under the surface $\partial\Omega^2$, which should therefore be orientable. The surface indexes 1 and 2 are arbitrary and can be exchanged. This condition can be reformulated even more easily as a relation between each surface point and the nearest points $\boldsymbol{r}_p$ of another surface:

$$\forall \boldsymbol{r}^1 \in \partial\Omega^1, \exists \boldsymbol{r}_p^2 \in \partial\Omega^2 \text{ s.t. } \forall \boldsymbol{r}^2 \in \partial\Omega^2,\ \|\boldsymbol{r}^1 - \boldsymbol{r}_p^2\| \leq \|\boldsymbol{r}^1 - \boldsymbol{r}^2\| \qquad [3.1]$$

Moreover, if the surface $\partial\Omega^2$ is sufficiently smooth, it can be said that for these points:

$$(\boldsymbol{r}^1 - \boldsymbol{r}_p^2) \cdot \boldsymbol{n}(\boldsymbol{r}_p^2) \geq 0$$

where $\boldsymbol{n}(\boldsymbol{r}_p^2)$ is the outgoing normal in the current configuration of point $\boldsymbol{r}_p^2$. If the surface, here $\partial\Omega^2$, is C^1-smooth, a normal vector can be uniquely defined at each point as:

$$\boldsymbol{n}(\boldsymbol{r}^2) = \frac{\frac{\partial \boldsymbol{r}^2}{\partial \xi^2} \times \frac{\partial \boldsymbol{r}^2}{\partial \eta^2}}{\left\| \frac{\partial \boldsymbol{r}^2}{\partial \xi^2} \times \frac{\partial \boldsymbol{r}^2}{\partial \eta^2} \right\|}$$

The parameterization of the surface ξ^2, η^2 must actually be chosen in such a way that the normal thus defined be outgoing. If these partial derivatives do not exist, the normal vector $\boldsymbol{n}$ cannot be uniquely defined. On the other hand, its derivatives can be defined using the notions of subdifferentials, and then defined as follows: the normal should be regarded as the set of normal vectors originating from the subdifferential of the surface at the point of interest (Moreau 1966; Heegaard and Curnier 1996; Pietrzak 1997; Yastrebov 2013). To simplify equation [3.1], the following notation is introduced:

$$g_n = g_n(\boldsymbol{r}^1, \partial\Omega^2) = (\boldsymbol{r}^1 - \boldsymbol{r}_p^2) \cdot \boldsymbol{n}(\boldsymbol{r}_p^2) \qquad [3.2]$$

where g_n is called the normal *gap*, whose absolute value defines the minimal distance between the point $\boldsymbol{r}^1$ and the surface $\partial\Omega^2$ if the latter is at least C^1-smooth (at least locally). The sign of g_n determines whether there is local penetration ($g_n < 0$) or separation ($g_n > 0$). We should bear in mind that in the general case, $g_n(\boldsymbol{r}^1, \partial\Omega^2)$ is not necessarily equal to $g_n(\boldsymbol{r}_p^2, \partial\Omega^2)$, where $\boldsymbol{r}_p^2$ is the closest point to $\boldsymbol{r}^1$ even if $\partial\Omega^1$ is C^1-smooth. With the definition of the normal *gap*, the contact conditions can be formulated as follows:

$$g_n \geq 0,\ \sigma_n \leq 0,\ g_n\sigma_n = 0 \qquad [3.3]$$

where $\sigma_n = \boldsymbol{n} \cdot \boldsymbol{\sigma} \cdot \boldsymbol{n}$ is the normal contact stress or the contact pressure negative $\sigma_n = -p$. Conditions [3.3] are called Hertz–Signorini–Moreau conditions (Wriggers 2006) or KKT (Karush–Kuhn–Tucker) in the convex analysis literature.

To give an example, consider a contact problem between a rough surface $\partial\Omega^1$ defined by $z(t, x, y)$ and an elastic half-space Ω^2 with the boundary $z = 0$. With no deformation, at each time instant, the gap is $g_n(\boldsymbol{r}^1, \partial\Omega^2) = z(t, x, y)$. However, in the current configuration, the gap is more complex because of the deformation of the half-space. It should be noted here, in the case considered and of a surface $z(x, y)$ nominally flat, that is, for any surface $S \subset \mathbb{R}^2$ large enough $\langle z \rangle = 0$, that when there are no external forces, $\forall \delta < \infty :\ z(t, x, y) = z(x, y) - \delta(t)$, the contact area remains zero.

This conclusion, which may seem surprising at first glance, is related to the Cheseaux–Olbers paradox (Harrison 1990): nonzero contact forces distributed over the surface of the elastic half-space with nonzero density create a nonzero average pressure over the entire infinite surface that results in infinite vertical displacement. Hence, if the displacement is finite $\delta < \infty$, the average pressure must be zero, so are the forces and the area of contact. A cleaner formulation would be to fix the rough surface $z(t, x, y) = z(x, y)$ and apply external pressure at infinity $-\sigma_{zz} = p_0$. In this example, the fraction of the contact area will be nonzero, regardless of the pressure applied.

NOTE.– The conditions [3.3] are strictly valid if and only if there is no fluid around the solids in contact. In real-life situations, a nonzero pressure fluid often surrounds bodies. To this end, to establish contact, the contact pressure must be greater than the fluid pressure everywhere at the edge of the contact zones $\forall \boldsymbol{r} \in \partial\mathcal{C} : \sigma_n \leq -p_f$, where p_f is the local fluid pressure. This correction is particularly relevant when contact pressure is comparable to fluid pressure (Shvarts and Yastrebov 2018a, 2018b).

NOTE.– At the macroscopic scale, it is sometimes assumed that the contact interface has a certain stiffness (Shi and Polycarpou 2005; Campañá et al. 2011; Pohrt and Popov 2012). This additional stiffness originates from the deformation of the roughness of both surfaces. At the macroscopic scale, if the surfaces are considered as averaged surfaces of the real surfaces (when there are no fine details), the actual contact can be established at a nonzero distance between averaged surfaces. On the other hand, the complementary stiffness must become infinite when the contact surface saturates and when in the contact area, the real contact area is equal to the contact area between average surfaces. This consideration justified the use of a barrier method with nonlinear parameters that captured the evolution of contact stiffness. Alternatively, a penalty method can be used to capture this complementary contact stiffness (Wriggers and Zavarise 1993; Andersson and Kropp 2008). However, in this case, the geometry of the surfaces should not be the average line of the actual surfaces but rather the surface that contains them and that exhibits the highest roughnesses. These techniques will not be physically justified in the context of small-scale contact because it is assumed that there is no longer any underlying roughness.

3.2.5. *Laws of friction*

There is a wide variety of friction laws which in their majority are nevertheless only relevant at the macroscopic scale. For example, Coulomb's law of friction according to which the tangential force $\boldsymbol{T}$ cannot exceed a threshold proportional to the normal force $\boldsymbol{N}$, that is, $\|\boldsymbol{T}\| \leq \mu\|\boldsymbol{N}\|$, can be considered as the consequence of the linear evolution of the local real contact area with the pressure $a \sim p$. According to the adhesive theory of contact (Rabinowicz 1965; Bowden and Tabor 1986; Straffelini 2001), the maximal resistance of asperities in contact to shear is given by a constant τ_c, then the maximal tangential force $T \leq \int a\tau_c dA \sim \int p\tau_c dA = \|\boldsymbol{N}\|\tau_c$. In sliding, in addition to dissipative losses on the surface, there exists dissipation present in the volume as it occurs with elastomers with viscoelastic behavior, metals with visco-elastoplastic behavior or the dissipation can originate from the formation of damage in any materials (micro cracks). At the macroscopic level, all of these energy losses are included in the law of friction. In addition, the heat produced near the contact interface alters the behavior of the material (thermal conductivity, Young's modulus, etc.) and can even cause phase change (glass transition, austenitization, melting, evaporation, etc.). All of these microscopic phenomena give rise to macroscopic friction laws (Vakis et al. 2018), which can be used for complex systems. The use of these laws at the roughness scale is confusing and cannot properly reproduce macroscopic friction laws. For this purpose, at the roughness scale, it is relevant to use Tresca-type friction laws, in other words, laws that assume

that the local tangential resistance does not depend on the local pressure (Krim 1996, 2002; Mo et al. 2009) and which can be formulated as follows:

$$\begin{cases} \|\boldsymbol{v}_t\| = 0, \text{ if } \|\boldsymbol{\sigma}_t\| < \tau_c \text{ adhesion} \\ \|\boldsymbol{v}_t\| > 0, \text{ if } \|\boldsymbol{\sigma}_t\| = \tau_c \text{ sliding} \end{cases} \quad [3.4]$$

where $\boldsymbol{v}_t$ is the tangential sliding speed, and $\boldsymbol{\sigma}_t = (\boldsymbol{I} - \boldsymbol{n} \otimes \boldsymbol{n}) \cdot \boldsymbol{\sigma}$ is the stress vector stripped of its normal component, that is, the stress vector in the tangent plane. To enhance the friction model, the dependency of the temperature and velocity threshold τ_c can be considered originating from the atomic scale (Gnecco et al. 2000; Gnecco and Meyer 2015):

$$\tau_c(T, v_t) = \tau_c^0 + \alpha T \log(v_t/v_0)$$

where α [Pa K^{-1}] is a constant related to the atomic structure and v_0 a normalization rate. However, at high speeds, thermal activation should no longer be significant and resistance should saturate. In the interval of these velocities, the following law can be used (Sang et al. 2001):

$$\tau_c(T, v_t) = \begin{cases} \tau_c^e - \alpha T^{2/3} \log(\beta T/v_t)^{2/3}, \text{ si } v_t < \beta T \\ \tau_c^e, \text{ if } v_t \geq \beta T \end{cases}$$

where α [Pa $\mathrm{K}^{-2/3}$] and β [m s^{-1} K^{-1}] are constants related to materials in contact.

The KKT conditions can thus be formulated as follows:

$$\|\boldsymbol{v}_t\| \geq 0, \ \|\boldsymbol{\sigma}_t\| - \tau_c \leq 0, \ (\|\boldsymbol{\sigma}_t\| - \tau_c) \|\boldsymbol{v}_t\| = 0 \quad [3.5]$$

Unlike Coulomb's law, this friction law is associative, which greatly simplifies how associated friction contact problems are addressed (Michalowski and Mróz 1978; Curnier 1984) because there is no coupling between contact pressure and shear. In addition, in the more general framework, Coulomb friction can be approximated by "fixed point"-based methods that make use of the Tresca law at each iteration (Panagiotopoulos 1975; Gwinner 2013).

NOTE.– Similarly to the way how penalization methods and barriers lose their physical motivation in the framework of small-scale normal contact of roughness, the same thing happens when addressing friction with the penalizationmethod, which should be avoided or utilized with particular caution, since there is no physical basis.

3.3. Finite element method

The FEM is a powerful and versatile tool for solving various problems in mechanics and physics (Bathe 1996; Zienkiewicz and Taylor 2000a, 2000b). However, contact remains a particular problem for this method because it requires the description of interaction between solids that each have their own discretization into finite elements. In the general case where the original surfaces are not geometrically compatible and/or their discretizations are not compatible either, processing contact remained a sensitive issue until recently. In this section, we will consider some questions of general interest in order to apply the FEM to micromechanical contact problems. All implementation details of contact algorithms can be found in the following monographs and doctoral theses: Kikuchi and Oden (1988); Pietrzak (1997); Laursen (2002); Wriggers (2006); Konyukhov and Schweizerhof (2012); Popp (2012); Yastrebov (2013); Akula (2019); Shvarts (2019).

Before covering the particularities of using FEM with microcontacts, we recall the basics of this method and its utilization for contact. The FEM is based on the principle of virtual works which, when there is no contact and in the infinitesimal context, can be described in the following form[5]:

$$\int_{\Omega} \boldsymbol{\sigma} : \delta\boldsymbol{\varepsilon} dV = \int_{\Omega} \rho(\boldsymbol{b} - \ddot{\boldsymbol{u}}) \cdot \delta\boldsymbol{u} dV + \int_{\Gamma_f} \boldsymbol{t}_0 \cdot \delta\boldsymbol{u}\, dS \qquad [3.6]$$

where $\delta\boldsymbol{u}$ denotes virtual displacements (or test displacements) that cancel out at the edges where Dirichlet conditions are prescribed Γ_u, that is, $\delta\boldsymbol{u} = 0$ on Γ_u, $\boldsymbol{b}$ are density forces, $\ddot{\boldsymbol{u}}$ is an acceleration vector, ρ is the density and $\boldsymbol{t}_0$ is the surface intensity of the prescribed forces on the Neumann surface Γ_f. The displacement $\boldsymbol{u}$ must verify the Dirichlet conditions $\boldsymbol{u} = \boldsymbol{u}_0$ on Γ_u and be in a functional space such that integrals in [3.6] make sense; this also applies to virtual displacements.

The introduction of contact constraints transforms the variational equality [3.6] into a variational inequality:

$$\int_{\Omega} \boldsymbol{\sigma} : \delta\boldsymbol{\varepsilon} dV + \int_{\Gamma_c} \boldsymbol{\sigma}_t \cdot \delta\boldsymbol{g}_t dS \geq \int_{\Omega} \rho(\boldsymbol{b} - \ddot{\boldsymbol{u}}) \cdot \delta\boldsymbol{u} dV + \int_{\Gamma_f} \boldsymbol{t}_0 \cdot \delta\boldsymbol{u}\, dS \qquad [3.7]$$

5 This form is called the weak form in contrast to the strong form because the former is obtained by the integration of the strong form, which allows, among other things, the conditions on the regularity of the solution to be weakened.

with the dissipation term put in the second integral evaluated on one side of the contact surface which remains unknown. At the same time, the solution $\boldsymbol{u}$ and the virtual displacement $\delta\boldsymbol{u}$ must verify the contact conditions $g_n(\boldsymbol{u}) \geq 0$ and $g_n(\boldsymbol{u} + \delta\boldsymbol{u}) \geq 0$. For friction laws relative to small scales [3.4], the friction dissipation integral can be reformulated as:

$$\int_{\Gamma_c} \boldsymbol{\sigma}_t \cdot \delta\boldsymbol{g}_t dS = \int_{\Gamma_{sl}} \tau_c \|\delta\boldsymbol{g}_t\| dS$$

where Γ_{sl} determines the sliding area in which $\|\sigma_t\| = \tau_c$. This form of the dissipative term preserves non-differentiability (Duvaut and Lions 1972; Kikuchi and Oden 1988) but eliminates the dependency of pressure.

In order to address the contact problem, inequality [3.7] (which can be thought of as a constraint optimization problem) can be transformed into an unconstrained optimization problem by means of classical methods such as the penalty method, the barrier method, the Lagrange multiplier method, the augmented Lagrangian method or using other optimization methods (Bertsekas et al. 2003). These methods can be used to remove the contact constraints imposed on the choice of real and virtual displacements and bring them back into the functional itself. After discretization of the continuous finite element formulation, a system of nonlinear equations is obtained that is generally solved using the Newton method in the implicit formulation of finite elements. This procedure naturally requires the linearization of the weak form (to obtain the tangent matrix), which is cumbersome in terms of implementation in the general case (Pietrzak 1997; Popp 2012; Yastrebov 2013). However, automatic bypass methods can lead to simplifying this procedure (Korelc 1997; Wriggers 2008; Lengiewicz et al. 2011).

Before moving on to the discussion of the applications of the FEM to small-scale contact problems, it would be important to make a few observations about the method itself.

3.3.1. *Convergence, parameters and loading step*

The convergence of the Newton iterations in contact problems cannot always be ensured for the given change of boundary conditions. However, the user can define control parameters such as the penalty coefficient(s) or the increase coefficient(s) in the augmented Lagrangian method. It is preferable that these parameters are defined independently for normal contact and tangential contact. In addition, it is also preferable that these parameters be independently defined for each localization, that is, for each contact element because these parameters are related to the local structural stiffness which is not uniform and which changes to nonlinear material

models. It is known that for the penalty method, the solution can be greatly impacted by to the choice of the penalty parameter.

It is therefore good practice to redo each calculation with the penalty twice as high, for example, which will make it possible to validate the solution. The practice of "naked eye" penetration control, in general, is never conclusive. The low penalization value often gives inaccurate results but ensures fairly rapid and robust convergence.

On the other hand, the high value of the penalization deteriorates the number of conditioning of the tangent matrix, which may be critical for iterative solvers and at the same time deteriorates convergence. For the augmented Lagrangian method, the choice of increase parameters does not influence the converged solution as much but how this solution (convergence itself) is reached strongly depends thereupon: a wrong choice of the increase parameter can easily result in an infinite convergence loop (Alart 1997; Yastrebov 2013). For optimal convergence, increase parameters can be adjusted on the fly during iterations (Bussetta et al. 2012; Sewerin and Papadopoulos 2017).

3.3.2. *Convergence of friction problems*

The convergence of quasi-static friction problems does not necessarily mean convergence towards the right solution. A striking example is the Hertzian contact between two cylinders or a plane and a 2D or 3D cylinder with Coulomb friction (see Figure 3.3). If the materials which the two solids are made of are different[6], introducing normal contact (without tangential forces) will produce shear stresses at the interface. On the other hand, the self-similar semi-analytic solution (Spence 1975; Johnson 1985) can be obtained if and only if the contact takes place in such a way that at each loading step very few elements come into contact.

It is however possible to reach the ultimate load in a single increment without convergence difficulty, but the solution obtained is different from the solution obtained for the same case achieved with 100 time steps (see Figures 3.3(d) and 3.3(e)) (Klarbring and Björkman 1992; Christensen et al. 1998; Kravchuk 2008; Spinu and Frunza 2015; Shvarts 2019). The importance of automatically choosing the loading step presents a relevant problem in contact mechanics that has only received very little attention (Torstenfelt 1984). Moreover, the solution of friction problems is not always unique, even theoretically in quasi-static special cases (Schatzman 1978; Klarbring 1990a, 1990b; Ballard 1999; Ballard and Basseville 2005).

6 More precisely, this statement is correct if the combination of the following elastic parameters $(1-2\nu_i)(1+\nu_i)/E_i$ is different for both materials (Johnson 1985).

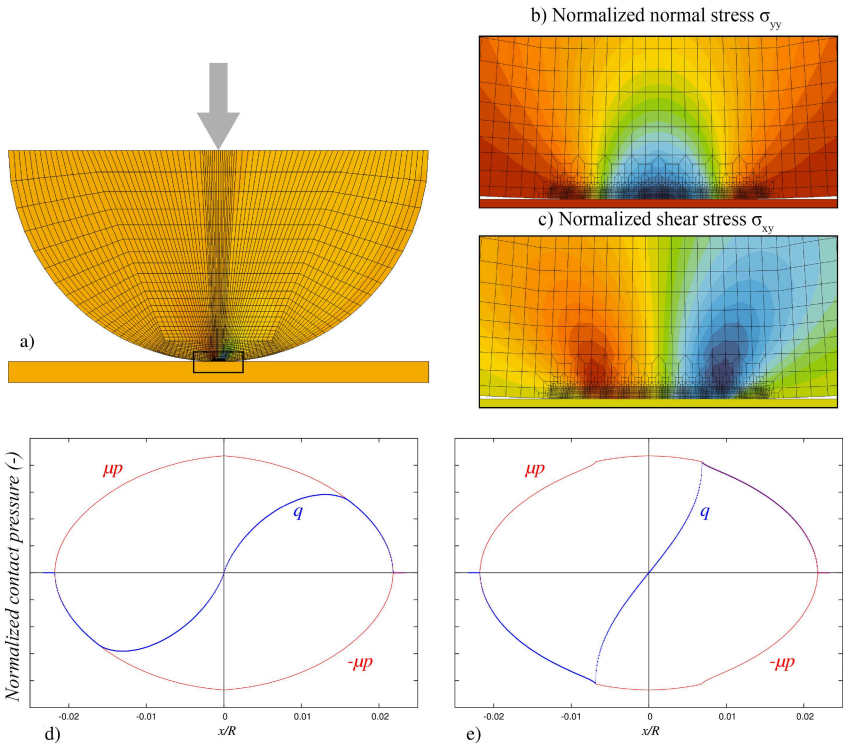

Figure 3.3. *Hertz problem with friction*

COMMENT ON FIGURE 3.3.– *Contact between an isotropic elastic half cylinder with a rigid plane under the displacement imposed on the upper surface of the cylinder (a). The magnified contact zone (b, c) demonstrates the distribution of normal stresses σ_{yy} and shear stress σ_{xy}, respectively, obtained with 100 loading steps with the imposed displacement following the parabolic form $u_y \sim i^2$, where i is the number of the time step. The stress distribution along the interface for this case is demonstrated in (d). For comparison, the distribution of the same forces for a solution obtained in a single loading step is demonstrated in (e), and this solution is erroneous. Figure is adapted from Shvarts (2019).*

The problem of elastodynamic friction is even worse in terms of solution existence and uniqueness. In the case of Coulomb friction between elastically different semi-spaces, the uniform sliding solution in the interface may be unstable. Even worse, the problem itself can be ill-posed. For example, in the case of friction between a rigid plane and an elastic half-plane, the problem remains well posed and there is an existing uniform slip solution for Coulomb friction coefficients of less

than one. On the other hand, for a coefficient of friction greater than one, the slightest stress disturbance at the interface grows exponentially in time with the exponent proportional to the wavenumber of this perturbation (Renardy 1992; Martins et al. 1995). Since there is no relevant wavelength limit in classical continuous mechanics, the problem becomes ill-posed and the lack of convergence with the mesh of these problems may lead researchers to erroneous conclusions (Andrews and Ben-Zion 1997). In problems with two deformable half-planes, the stability of the solution depends on the contrast of their elastic properties and their densities (Adams 1995; Cochard and Rice 2000; Ranjith and Rice 2001): there are situations where the stable solution exists but only for friction values below a certain critical threshold, and there are cases where the solution is unstable or ill-posed, regardless of the coefficient of friction. These instabilities are related to the strong coupling between contact pressure and shear stress in the case of different materials. These effects give rise, for example, to brake squeal noise (Kinkaid et al. 2003; Massi et al. 2007) and slip localizations in geological faults that are responsible for earthquakes (Heaton 1990). For finite-sized or stratified systems, uniform slip can always be unstable (Brener et al. 2016; Mohammadi and Adams 2018), which manifests itself in slip spatio-temporal localization (Renard 1998; Adams 2000; Bui and Oueslati 2010), adhesion and even opening in some cases (Gerde and Marder 2001; Moirot et al. 2003; Yastrebov 2016). To meet this challenge, studies of friction dynamics must reject Coulomb-type laws where the shear stress is proportional to the contact pressure. This bond can be softened by a viscoelastic type relationship as can be seen in the Prakash–Clifton law of friction, which is based on an experimental observation (Prakash and Clifton 1993; Prakash 1995) of non-immediate friction adjustment in response to an instantaneous pressure change. This regularization of friction results in obtaining physical and converged results (Cochard and Rice 2000; Ranjith and Rice 2001; Kammer et al. 2014). An alternative is the use of nonlocal friction laws (Simoes and Martins 1998). However, for relevant friction laws at the roughness scale, friction dynamics must not represent the following defects due to the absence of normal-tangential stress coupling.

3.3.3. *Quadratic convergence*

Unlike many nonlinear problems in continuous media mechanics, contact problems in most cases do not quadratically converge with the Newton method. This lack of quadratic convergence is caused by the change in status of the contact elements between contact/noncontact and slip/adhesion. If the set of statuses is fixed, the convergence becomes quadratic when all of the terms of the tangent matrix have been included. In contact problems with the very rapid change of boundary conditions (e.g. initial penetration greater than element size), it is preferable not to include all terms in the tangent matrix, which can be added as soon as the convergence of statuses occurs (Wriggers 2006).

3.3.4. *Mesh and computation time*

The stress state considerably varies near the contact area which therefore requires fine meshes in these areas to ensure the accuracy of the digital solution. The contact pressure near the edge of the contact area within the framework of smooth surfaces changes as $p \sim t^{1/2}$, where t is the distance to the edge. Because of this fast decreasing contact pressure, the very fine mesh is necessary to be able to determine the boundary between contact and noncontact and to measure the contact area, which is important for a large number of micromechanical contact problems (Yastrebov et al. 2017a, 2017b). For flat punches, the pressure near the edge evolves as $p \sim t^{-1/2}$. In this case, it is easy to refine the mesh near this edge that is a priori known. On the other hand, for a sliding contact, the uniformly fine mesh would be necessary for this problem. Mesh refinement is also necessary if the coefficient of friction is not continuous along the contact interface (Ballard 2016) or when studying a mode II or III crack. In all of these cases, constraint singularities appear at the interface (Coker et al. 2005; Svetlizky and Fineberg 2014; Barras et al. 2014; Kammer et al. 2015; Svetlizky et al. 2016).

The simulation of the contact between nonlinear materials requires refined volume meshes near contact zones (Nigro et al. 2014). This is the case in studies of the behavior of isolated asperities that will be discussed in detail in section 3.4 where mesh refinement is very important for detecting the initiation of the plasticization process that begins in the volume when there is no surface friction (Johnson 1985; Hill et al. 1989; Mesarovic and Fleck 1999; Kogut and Etsion 2002), but also for obtaining a precise macroscopic force–displacement response that strongly depends on the fineness of the volume mesh. This requirement on mesh fineness incurs a bottleneck in computing rough surfaces in contact with the FEM even when using very advanced parallel methods deployed on high-performance computing clusters (Dostál et al. 2016), because it involves very high computation times. In addition, in order to conduct a statistically significant study of contact between rough surfaces, a very large number of calculations must be performed (Yastrebov et al. 2015; Rey et al. 2019). Nonetheless, the fine mesh can be restricted to the area near the contact interface only and remain coarse enough away from this area to simply capture the stiffness of the system or avoid edge effects. Some examples of such meshes are shown in Figure 3.4.

3.3.5. *Contact constraint*

In contact problems, the focus is often on the distribution of surface stress. However, this is not always easy to achieve because the constraint is often evaluated at the integration points located inside the elements. In order to have nodal values and use interpolation later, finite element software programs extrapolate the values found at the points of interest and averaging. The direct consequence of this procedure is that the contact stress obtained in such a way is not very accurate and may have nonzero values outside the contact area. To recover true stress values, the stresses

must be found at the surface using directly $\boldsymbol{\sigma} = \boldsymbol{C} : (\nabla \boldsymbol{u} + \boldsymbol{u}\nabla)/2|_{\boldsymbol{x}\in\Gamma_c}$ in the elastic case, where $\boldsymbol{C}$ is the fourth-order elasticity modulus tensor, this calculation could be done during *post-processing*. For nonlinear materials involving state variables, the surface stress computation procedure is more costly and requires the addition of surface integration points at the very beginning of the computation and involves the integration of the material model locally (Simo and Hughes 1998). Contrary to what may appear to be the case, this discussion is as relevant for using the conventional penalization method as it is for the Lagrange multiplier method. It is true that in the latter it is more trivial to have values of the contact forces (forces [N]), which are represented by Lagrange multipliers in node-to-surface discretization. For this purpose, in order to determine stresses [N/m^2], it is necessary to associate an area with each surface node to normalize the value of the Lagrange multipliers. Although performing this procedure in 2D is trivial, this is not what happens in 3D. Another possibility to have a good estimation of surface stresses is to have a thin layer of the elements near the contact surface to minimize extrapolation error. In state-of-the-art methods, surface stresses can be directly obtained, these are surface-to-surface type discretization methods: mortar and Nitsche methods (Belgacem et al. 1999; Puso and Laursen 2004; Puso et al. 2008; Wriggers and Zavarise 2008; Popp et al. 2010; Temizer et al. 2012; Chouly and Hild 2013; Chouly et al. 2015).

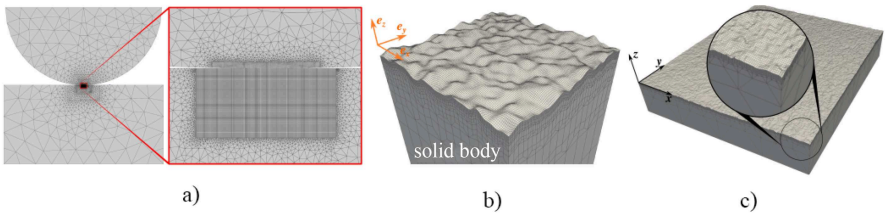

Figure 3.4. *Finite element meshes for (a) 2D fatigue fretting contact (source: Sun 2012); (b and c) rough contact with roughness (source: Shvarts 2019)*

It is important to notice that node-to-surface methods cannot transfer uniform surface forces between non-compliant meshes, which represents a "patch-test" of interface problems (Taylor and Papadopoulos 1991) (see Figure 3.5). This effect is related to the under-integration of contact stresses at the interface from which the advanced analysis was derived to meet this challenge (Crisfield 2000; El-Abbasi and Bathe 2001; Tan 2003; Chen and Hisada 2006; Hartmann et al. 2009; Oliver et al. 2009; Zavarise and De Lorenzis 2009a, 2009b). Despite that parasitic oscillations due to subintegration might have very small amplitudes, they can lead to erroneous solutions if we are focusing on the surface stress state and if, for example, wear laws based on these stresses are used to update the geometry of worn surfaces (Lengiewicz and Stupkiewicz 2013; Basseville and Cailletaud 2015; Farah et al. 2016; Basseville et al. 2019). Surface-to-surface type methods can be used to avoid this defect and

ensure an accurate stress state. However, if the contrast between materials is very high, then similar oscillations may appear in the contact even with these methods (Akula et al. 2019).

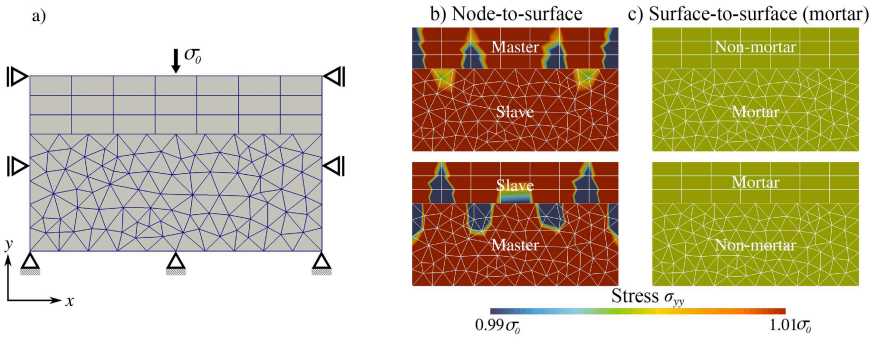

Figure 3.5. *Comparison of normal stresses σ_{yy} with (b) node-to-surface (NTS) and (c) surface-to-surface (STS) discretization for different choices of master-slave and mortar/non-mortar surfaces with NTS and STS, respectively (adapted from Akula 2019)*

3.3.6. *Surface regularity*

Naturally, finite element surfaces are of regularity class C^0 (only continuity), even if they are C^∞-smooth inside the regions of the elements. The incompatibility of gradients at the junction between elements is related to the compact nature of finite element shape functions. This irregularity in surface geometry poses problems for addressing contact because it induces oscillations in local stresses that can result in macroscopic oscillation of forces.

To avoid these problems, in applications of contact between bodies of very different stiffness (tire/road, hardness test indenter/substrate, touch screen/finger and shoe/floor), it is preferable to use rigid surfaces described by analytical functions or CAD models (Heege and Alart 1996): the simplest example would be a rigid plane, which is widely used in micromechanical contact for isolated asperities as well as for rough surfaces (Mesarovic and Fleck 1999; Kogut and Etsion 2002; Pei et al. 2005; Yastrebov et al. 2011). However, the iso-geometric analysis (IGA) method, which takes advantage of smooth and at the same time deformable surfaces, makes it possible to forget the issues of surface regularity.

However, the formulation of the contact in the context of the IGA is not direct because the too regular nature of the solutions does not allow the representation of the contact pressure, which reaches a zero with vertical slope. To this end, different

techniques have been developed and can be found in the review articles by Temizer et al. (2011); De Lorenzis et al. (2014).

In the context of classical finite elements, smoothing techniques can be utilized: this can either exclusively concern the normal vector field (Yang et al. 2005; Popp et al. 2010), or directly surface geometry (Wriggers and Krstulović-Opara 2000; Wriggers et al. 2001; Belytschko et al. 2002; Puso and Laursen 2002; Chamoret et al. 2004; Munoz 2008). In addition, the FEM with additional degrees of freedom of rotation, which ensures the regularity of the normal at the junctions of the elements, can be considered as an alternative solution to smoothing (Batailly et al. 2013).

UNINTERRUPTED FRACTAL SURFACE.– A contact problem between rough surfaces with a high-frequency uninterrupted self-affine spectrum (see, for example, Hyun et al. 2004; Pei et al. 2005) presents a problem poorly posed from a numerical mechanics point of view. Since the shortest surface wavelength is limited by the size of the element, convergence cannot be achieved by refining the mesh, which of course also poses the problem of interpreting the computational results.

3.4. Application I: study of an isolated asperity

3.4.1. *Elastic asperity*

In the continuous and smooth description[7] of "rough" surfaces, "asperities" can always be isolated, namely, the elements of the simple geometry that can be locally approximated by elliptical paraboloids:

$$z(x,y) = \frac{x^2}{2R_x} + \frac{y^2}{2R_y} + z_0$$

in an orthonormed basis $\{x, y\}$ with two principal radii of curvature R_x, R_y such that $R_x R_y > 0$. However, crystal (minerals) surfaces can be described by different elementary shapes such as steps, ridges and pyramids. It should be noted that apart from paraboloids, which are essential for the study of weak contact, another quadric – hyperbolic paraboloid or saddle point ($R_x Ry < 0$) – is essential for the study of critical junctions in runoff problems between rough surfaces in contact (Plouraboué et al. 2004; Dapp et al. 2012; Dapp and Müser 2016; Shvarts and Yastrebov 2018a) but also for contact beyond the infinitesimal area hypothesis (Johnson et al. 1985; Yastrebov et al. 2014).

7 If the surface is smooth, it is automatically *non-fractal* because fractals are not differentiable manifolds: elements of these surfaces cannot be described by simple and differentiable shapes.

The study of contact between rough edges represents an important branch of the study of microscopic contacts. First of all, it should be noted that this type of contact is directly related to the indentation study, especially if the asperities are described at the scale where the classical theories of continuous media remain valid. On the other hand, at a small scale, where the purely local characterization of the deformation ceases to be valid, the link between the contact of asperities and micro- or nano-indentation should rather be considered. The objective of this section is to present a review of studies of these elementary contacts carried out with the finite element or boundary method. At the same time, in relevant cases, we will highlight numerical innovations that have been used.

The problem of purely linear elastic contact between elliptical paraboloids represents the first study of deformable contact which was carried out by Hertz (1881). In the simple case of revolution surfaces, the contact radius a, the gap δ and the contact pressure distribution are found:

$$a = \left(\frac{3NR^*}{4E^*}\right)^{1/3} \qquad [3.8]$$

$$\delta = \frac{a^2}{R^*} = \left(\frac{9N^2}{16R^*E^{*2}}\right)^{1/3} \qquad [3.9]$$

$$p(x,y) = \frac{3P}{2\pi a^2}\sqrt{1-\frac{x^2+y^2}{a^2}} \qquad [3.10]$$

where N is the normal force, $R^* = R_1R_2/(R_1+R_2)$ is the effective radius of curvature with R_i being the radius of curvature of the surface $i = \{1,2\}$, $E^* = E_1E_2/[(1-\nu_2^2)E_1 + (1-\nu_1^2)E_2]$ is the effective modulus of elasticity with ν_i, E_i is the Poisson coefficient and Young's modulus of the field $i = \{1,2\}$. In the vicinity of the vertex, the parabolic surface $z = r^2/(2R)$ is equivalent to a spherical surface $z = R - \sqrt{R^2 - r^2}$ up to $o(r^2/R^2)$. To this end, the Hertz theory formulated for paraboloids works just as well for spheres if $a/R \ll 1$.

Now, Hertzian contact is the conventional test for validating numerical contact processing techniques. However, these validation tests are often limited to validating the method for two-dimensional surfaces of revolution $R_x = R_y$ with respect to the axial symmetry of the problem. The simplest validation can be made for the contact between a rigid plane $R_1 = \infty$, $E_1 = \infty$ and a deformable paraboloid (sphere or its half) $R_2 = R^*$, $E_2 = E^*(1-\nu_2^2)$. On the other hand, an axisymmetric representation may be satisfying only in the case of normal contact (with no tangential loading).

CALCULATION OF THE CONTACT AREA.– Since the computation of the contact area or contact radius is based on the calculation of the number of contact areas/elements, the numerical evaluation of the contact area is not continuous: the contact radius grows by steps of comparable size to the discretization of contact surfaces $\Delta a \lessapprox h$, which therefore determines the numerical error of the contact radius. In the general case, as this error is located at the perimeter P of the contact region of area A, the error on the contact area depends on the ratio $E_r \sim Ph/A$ that for the revolution contact is reduced to $E_r \sim 2h/a$, which explains the need for very fine meshes near the contact boundary to correctly capture the contact area. For rough surfaces with the minimal wavelength λ_s, the curvature of the asperities $R \sim \lambda_s^2/(4\pi^2\Delta)$, where Δ is the amplitude related to this wavelength. Given that $a \sim \sqrt{R^*\delta}$, the computation error of the contact area evolves as $E_r \sim \frac{4\pi h}{\lambda_s}\sqrt{\frac{\Delta}{\delta}}$ for each asperity in contact whose number can be very large (Yastrebov et al. 2017a; Shvarts 2019).

Apart from this simple case which is exclusively used to validate numerical methods, the contact interaction can be enhanced with friction and/or adhesion. In the presence of friction, the analytical solution exists only for the following three cases: (1) normal and tangential contact between identical materials (see footnote 6, in section 3.3.2) or noncompressible materials; (2) normal contact with infinite friction (Mossakovskii 1954, 1963; Abramian et al. 1966; Spence 1968); and (3) stationary slip asperity (Goodman and Hamilton 1966; Hamilton 1983). These three cases can be used to validate the implementation of friction contact algorithms. The most used and richest case of the three is notably the case of contact between two similar materials that was derived in Cattaneo (1938); Mindlin (1949). This test was used in Laursen and Simo (1993); Yang et al. (2005); Gitterle et al. (2010); De Lorenzis et al. (2011); Wei et al. (2016); Akula et al. (2019) to name some. Another friction test was used in Alart and Curnier (1991); Yastrebov (2013) based on a semi-analytical solution of Klang (1979). The test consists of a contact between a cylinder and a circular hole in a plane that have quasi-conformal geometries. Nevertheless, the two numerical solutions (Alart and Curnier 1991; Yastrebov 2013), which agree, do not converge to the analytical solution in terms of shear stress distribution. A more consistent numerical solution was obtained in Pietrzak and Curnier (1999) for a slightly different geometry than that used in the two attempts mentioned above.

3.4.1.1. *Normal and tangential contact separability*

In the general case, the contact problem can be divided into two decoupled problems (normal contact and tangential contact problems) if and only if the elastic constants of two bodies in contact are the same (see footnote 6, section 3.3.2) and when the edges or interfaces are far enough from the contact area. Otherwise, the two problems remain coupled and cannot be rigorously solved separately. However, still with the same material, numerical schemes need to be used with great caution

to obtain correct results even for normal loading; see examples of erroneous solutions (Andersson 1981, appl. 1; Shyu et al. 1989). The coupling between tangential forces $\tau(x)$/normal $p(x)$ applied to $x \in (-b, a)$ and the associated displacements v, u can be explicitly visualized by the shape of the fundamental Flamant and Cerutti solution for an elastic half-plane (Johnson 1985):

$$\left.\frac{\partial u_i}{\partial x}\right|_{y=0} = -\frac{(1-2\nu_i)(1+\nu_i)}{E_i}p(x) - \frac{2(1-\nu_i^2)}{\pi E_i}\int_{-b}^{a}\frac{\tau(s)}{x-s}\,ds \qquad [3.11]$$

$$\left.\frac{\partial v_i}{\partial x}\right|_{y=0} = \frac{(1-2\nu_i)(1+\nu_i)}{E_i}\tau(x) - \frac{2(1-\nu_i^2)}{\pi E_i}\int_{-b}^{a}\frac{p(s)}{x-s}\,ds \qquad [3.12]$$

where $i = 1, 2$ designates the values associated with the ith body.

A semi-analytic solution for a problem involving a rigid indentor based on the consideration of self-similarity was obtained by Spence (1975). It should however be noted that self-similarity is lost on unloading (Stingl et al. 2013; Kim and Jang 2014). This problem, generalized to the case of two deformable solids (Nowell et al. 1988), represents a reference test for the implementation of friction contact algorithms (Jinn 1989; Klarbring and Bjöourkman 1992; Christensen et al. 1998; Guyot et al. 2000; Gallego et al. 2010; Akula et al. 2019). This normal contact with no coupling between normal and tangential tractions was considered in Hills and Sackfield (1987). However, we need to bear in mind that this decoupling is exclusively feasible with the boundary element method and cannot be used with finite elements where coupling is inherent. We can note that examples of false numerical solutions of this problem are recurringly found in the literature; as examples see Jing and Liao (1990); Lee (1994); Kosior et al. (1999); Elkilani (2003); Li and Berger (2003); Chen and Wang (2008) and see a discussion on the subject in Kwak and Lee (1988). The self-similarity of the solution can be used to speed up numerical computations by reducing the calculation to a single loading step with additional conditions to be verified (Storåkers and Elaguine 2005; Jelagin and Larsson 2012).

In addition to being used as a test case for numerical algorithms, this problem of normal contact between different bodies is also important for several applications, especially to understand failure modes (wear and fatigue crack initiation) of micro- and macroscopic cyclic normal contact.

Another test that involves compression and torsion of the contact area with finite friction between a rigid plane and a deformable sphere was used in Chaudhary and Bathe (1986) based on an analytical solution (Hetenyi and McDonald 1958). This

problem involves a normal loading phase with no friction that is followed by a torsion phase with finite friction. This hypothesis is non-physical because the influence of history is precisely what makes the friction problem so complex and it is not taken into account in this solution. Another numerical test for frictional contact between a deformable body and a rigid indenter is the axisymmetric indentation of an elastic half-space by a cylindrical punch whose solution has been shown to be similar to parabolic indentation (Spence 1975): this problem was used to test the implementation of augmented Lagrangian in Torstenfelt (1984); Pietrzak and Curnier (1999); Yastrebov (2013). An automation of the choice of loading step for friction problems was proposed in Torstenfelt (1984).

This section will be concluded by highlighting the lack of analytical and numerical solutions for normal and tangential contact between paraboloids made up of similar or different materials with a Tresca-type friction law that is more relevant at a small scale of asperities than Coulomb's law.

3.4.2. *Elastoplastic asperity*

The elastoplastic behavior of the material in the vicinity of contact zones is highly relevant for many engineering applications that involve metallic materials. From the force–displacement curves of a hard indentor (diamond or tungsten carbide) on a metallic material or based on the impression, several properties of the material can be found (Tabor 1951; Oliver and Pharr 1992; Fischer-Cripps 2011; Herrmann et al. 2011). The relevance of this type of indentor/substrate interaction is obvious for microscopic contact: at a small scale, asperities of the harder ("less plastic") material can be seen as indentors for the asperities of the other material. Understanding the normal and tangential interaction of parabolic surfaces in the elastoplastic regime is necessary for understanding the microscopic contact of metals and alloys. In this section, we briefly review the numerical calculations of elastoplastic contact either between a rigid parabolic/spherical indenter and a deformable substrate, or the opposite, or between both deformable bodies.

Many studies dedicated to elastoplastic contact focus exclusively on the loading phase. However, the unloading phase as well as repetitive contact (cyclic loading) are very important to consider for asperity contact. Figure 3.6 shows the results of a finite element calculation of the elastoplastic behavior of a spherical body under cyclic loading where each new cycle has a higher loading amplitude than the previous cycle. The zero cycle is purely elastic and follows the Hertz solution. For cycles with a higher force (branch 1), the contact pressure saturates with the hardness of the material and the derivative of the contact area A with respect to the compressive force $\partial A/\partial F$ remains constant, that is, the contact area evolves in an affine manner with the force $A = A_0 + F/H$, where H indicates the hardness of the material. The constant A_0 is often neglected because it can be very small for developed plastic contact. Unloading

(branch 2), in this case, is completely elastic, but does not follow the Hertz solution $A \sim F^{2/3}$ because the residual curvature is not constant at all points as it should be for the Hertz solution to be valid. The consecutive reloading, branch 3, again follows branch 2 (since we still are in the frictionless elastic regime), but as soon as the load exceeds the maximum load of the previous cycle, the solution qualitatively changes and again follows the saturation curve (branch 4) and so on: elastic unloading (5); elastic reloading (6), saturation under load (7). It is therefore clear with this example that the contact area cannot be predicted for a given load because the loading history is involved as in all nonconservative evolving problems.

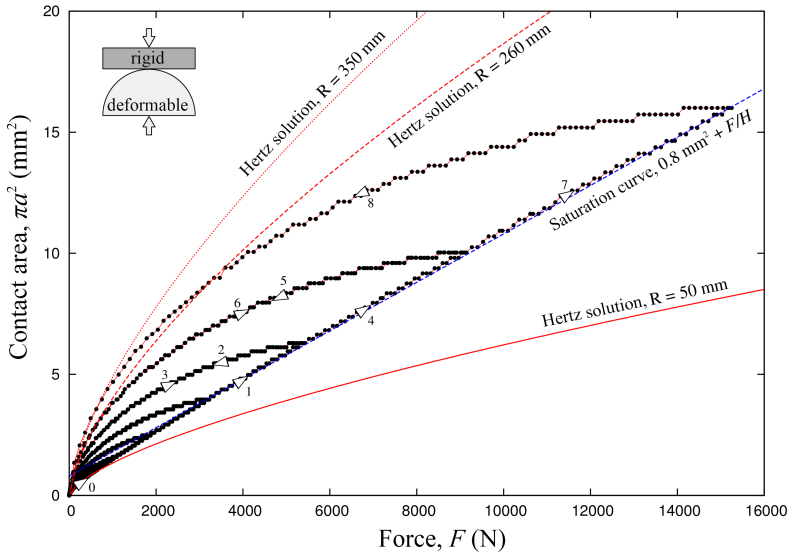

Figure 3.6. *Cyclic loading of an elastoplastic "asperity" of the initial radius R = 50 mm in contact with a rigid plane*

Many studies on elastoplastic indentation have been performed and include Komvopoulos (1989); Kral et al. (1993); Song and Komvopoulos (2013) as well as Kogut and Etsion (2002, 2003a); Etsion et al. (2005); Kadin et al. (2006); Brizmer et al. (2007). The elastoplastic contact in the presence of coating was studied in Sun et al. (1995); Song et al. (2012) using the FEM.

In an idealized case of normal contact between parabolic surfaces and with no friction and adhesion, the Hertz theory makes it possible to predict the beginning of plastic flow. To obtain the start point located on the axis of symmetry, the von Mises stress σ_{eq} for

example, simply has to be differentiated with respect to the normalized depth $z' = z/a$ where a and the contact radius. Using the following equations:

$$\frac{\sigma_z(z)}{p_0} = -\frac{1}{1+z'^2} \quad [3.13]$$

$$\frac{\sigma_r(z)}{p_0} = \frac{\sigma_\theta(z)}{p_0} = (1+\nu)\left(z'\arctan(1/z') - 1\right) + \frac{1}{2(1+z'^2)} \quad [3.14]$$

and the von Mises stress is given by:

$$\sigma_{\text{eq}} = |\sigma_z - \sigma_r| = p_0 m(\nu, z') \quad [3.15]$$

with:

$$m(\nu, z') = \left|(1+\nu)\left(1 - z'\arctan(1/z')\right) - \frac{3}{2(1+z'^2)}\right|$$

It can then easily be shown that the von Mises stress reaches the maximal value at a distance z'^* which verifies $\partial\sigma_{\text{eq}}/\partial z' = 0$. The last equation is reduced to the following equation:

$$(1+\nu)\left(\arctan(1/z'^*) - z'/(1+z'^{*2})\right) = 3z'/\left(1+z'^{*2}\right)^2 \quad [3.16]$$

The solution to this equation can be approximated by an affine function (see Figure 3.7(b.4)):

$$z'^* \approx 0.3819375 + 0.33187\nu \quad [3.17]$$

Then, the function $m(\nu, z'^*)$ can be approximated by another affine function (see Figure 3.7(b.3)):

$$\max(\sigma_{\text{eq}}/p_0) = m(\nu, z'^*) \approx 0.7696422 - 0.4738901915\nu \quad [3.18]$$

Finally, if the yield strength is given by σ_Y, then maximal pressure at the center of the contact p_0^* needed to initiate plasticization is given by p_0^* and the depth is given by z^*, respectively:

$$p_0^* = \frac{\sigma_Y}{m(\nu, z'^*)},\ z^* = z'^* a^* = \frac{\pi z'^* p_0^* R^*}{2E^*} = \frac{\pi z'^* \sigma_Y R^*}{2E^* m(\nu, z'^*)}$$

where R^* is the effective radius of curvature, and E^* is the effective modulus of elasticity. From these equations, the onset of the normalized depth of plastic flow can be found approximately using [3.18] and [3.17] (Figure 3.7(b.2)):

$$\frac{z^*}{R^*} \approx \frac{1,199892 + 1,042600\nu}{1,53928444 - 0,947780\nu} \frac{\sigma_y}{E^*} \qquad [3.19]$$

If assuming that the indenter is rigid, it follows that the effective modulus of elasticity depends only on the Poisson coefficient of the deformable solid $E^* = E/(1-\nu^2)$, which gives us the following approximate form for the normalized depth of the onset of plasticity (Figure 3.7(b.1)):

$$\frac{z^*}{R^*} \approx \frac{(1.199892 + 1.042600\nu)(1-\nu^2)}{1.53928444 - 0.947780\nu} \frac{\sigma_y}{E} \qquad [3.20]$$

This analytical estimate is used to build a finite element mesh adapted to elastoplastic calculations, in other words, to have the depth of the fine mesh that would be adapted to the calculation. It should noted that the onset of plasticity cannot be easily detected during the indentation test because if the plastic area remains very small, then it does not affect the loading curve.

Box 3.1. *Onset of plasticity*

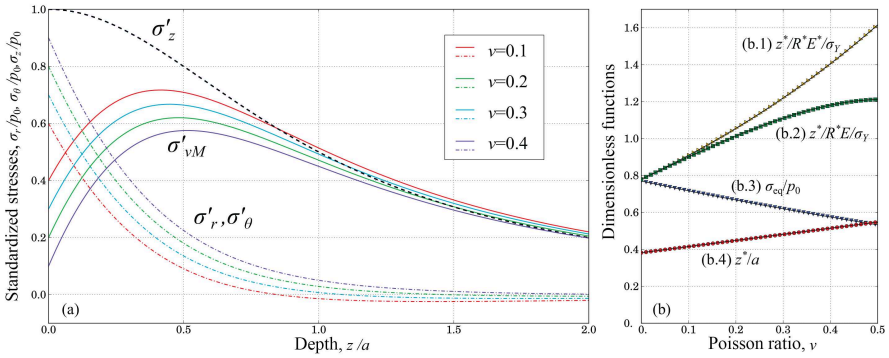

Figure 3.7. *Stress under Hertzian contact*

COMMENT ON FIGURE 3.7.– *(a) Stress σ_θ, σ_r and σ_z along the axis of symmetry; (b) dimensionless functions which represent: (b.1) the normalized depth of plastic flow*

onset $z^*/R^*E^*/\sigma_Y$, (b.2) the normalized depth with the rigid indenter $z/R^*E/\sigma_Y$, (b.3) the maximal normalized von Mises stress σ_{eq}/p_0, (b.4) the normalized depth z^*/a, the solution to equation [3.16]; The solid lines in (b) represent approximate solutions [3.19], [3.20], [3.18], [3.17], respectively.

Of course, with small-scale roughness, the microstructure of the metal must be taken into account because the von Mises plasticity model is not very relevant at this scale. Nevertheless, hardness and force–displacement curves are not very affected by CFC crystal plasticity (namely crystallographic orientation) because many slip systems are activated (Casals and Forest 2009; Durand 2012; Sabnis et al. 2013). This is however not the case for the HCP network (Casals and Forest 2009). However, the morphology of the plastic area is very sensitive to the crystallographic orientation of the indented crystal. In addition to crystal plasticity anisotropy, elastic anisotropy must be taken into account at this scale. Since even the Boussinesq-based solution cannot be analytically obtained in the case of general anisotropy, the solution to the contact problem between anisotropic bodies is a difficult problem. It was, however, solved by Willis (1966, 1967) through the use of Fourier transforms, where the problem is reduced to the numerical evaluation of contour integrals. The two-dimensional case is simpler and there are analytical methods to address it (Lekhnitskii 1981).

The direct calculation of the depth of the onset of plasticity for very small curvature radii yield values comparable to interatomic distances. Consider polycrystalline gold which has yield strength $\sigma_Y = 140$ MPa, modulus of elasticity $E = 79$ GPa, Poisson coefficient $\nu = 0.4$, CFC crystalline parameter $a = 0.4$ nm. The onset depth can be estimated based on equation [3.20] at $z^* \approx 0.0021R^*$. When a gold surface is indented by a harder asperity of micrometric radius, the depth z^* is nanometric, for $R^* = 1$ μm, $z^* \approx 2.1$ nm $= 5.25a$, which cannot be properly described in the context of continuous media mechanics and isotropic plasticity. At this scale, the discrete nature of the crystal lattice must be taken into account, as in the following multi-scale studies (Fivel et al. 1998; Chang et al. 2010). Under the high pressure, at this small scale, the pressure saturates with the hardness of the material, which in turn depends on the scale (either the depth of the indentation for non-smooth indenters (Nix and Gao 1998; Qiu et al. 2001; Feng and Nix 2004), or the radius of curvature for spherical indenters (Swadener et al. 2002; Gao et al. 2015)). Through geometric (accommodation of shape by geometrically necessary dislocations) and phenomenological considerations (based on the saturation of dislocations), simplified laws for contact hardness H were deduced. The simplest distribution for a conical indenter takes the following form Nix and Gao (1998):

$$\frac{H}{H_0} = \sqrt{1 + \frac{d_0}{d}} \qquad [3.21]$$

where the macroscopic hardness is H_0, d is the indentation depth and d_0 is an internal distance characterizing the material. A more elaborate law has been proposed in

Qiu et al. (2001) and Feng and Nix (2004), which takes into account the high frictional stress that is characteristic of body-centered cubic (CC) crystals:

$$\frac{H - H_P}{H_0 - H_P} = \sqrt{1 + \frac{1}{(1 + \beta \exp(-d/d_1))^3}}\ \frac{d_0}{d} \qquad [3.22]$$

where $H_P = 3\sqrt{3}\ \tau_P$ and where τ_P is the Peierls stress, $1 + \beta \exp(-d/d_1) = r/a(d)$ represents the ratio between the radius of extension of the plastic zone with respect to the contact radius $a(d)$, which is a sinking function d, H_0 is the macroscopic hardness, and d_1, d_0 are characteristics of the material.

In the case of a spherical/parabolic indenter, the depth of sinking no longer modifies the material hardness, but the radius of curvature of the indentor R does. The simple model and, unlike conical indentation, without adjustable parameters, can be proposed in this case (Swadener et al. 2002):

$$\frac{H}{H_0} = \sqrt{1 + \frac{R_0}{fR}} \qquad [3.23]$$

where $R_0 = \bar{r}/(\rho_s b)$, and $\bar{r}$ is the Nye factor[8], ρ_s is the density of statistical dislocations in the deformed region, b is the Burgers vector, and the factor f is the ratio of the imprint curvature radius to the indentor radius that can be taken approximately $f = 1.17$ (Swadener et al. 2002). For gold, $b = 0.288$ nm, the statistical density of dislocations in the strongly deformed region under the indenter can be estimated as $\rho_s \approx 10^{16}$ m^{-2}, and for the Nye factor $\bar{r} = 2$, we get $R_0 \approx 0.69$ μm, which agrees with Kim et al. (2018). For macroscopic hardness $H_0 = 250$ MPa, we obtain the following hardness:

$$H = 250 \text{ MPa} \sqrt{1 + \frac{0.59\ \mu\text{m}}{R}}$$

Clearly, this equation cannot be used in finite element calculations, but it can be used in calculations made with multi-asperity models (Kogut and Etsion 2003a; Ciavarella et al. 2006; Afferrante et al. 2012; Yastrebov 2019) or with boundary element codes involving the phenomenological consideration of plasticity by contact pressure saturation (Sahlin et al. 2010; Manoylov et al. 2013). To simulate the size effect with finite elements, generalized models of the continuous medium

8 The Nye dimensionless factor determines the fraction of dislocations that must be created to accommodate the plastic strain relative to the number of geometrically necessary dislocations.

(Forest 1998; Maugin and Metrikine 2010; Altenbach et al. 2011; Eringen 1999) should be used, as in Zhang et al. (2005); Zisis et al. (2014); Song et al. (2017); Lewandowski and Stupkiewicz (2018).

With friction, the von Mises stress can be quite high at the surface and it can therefore create another source of plasticity growth that will aggregate at the plastic core developed below the surface. The effect of friction on indentation was discussed in several works (Tabor 1951; Mata and Alcala 2004), even if the discussion is limited to Coulomb's law which can be imprecise in indentation[9] and is not valid at a small scale. In addition, very high pressures are frequent in other applications such as, for example, indentation, machining (Özel 2006) or metal forming and rolling (Wilson and Sheu 1988; Ma et al. 2010; Hol et al. 2012). In some studies, the effect of friction is included in the analysis by considering two borderline cases: frictionless and with infinite friction, that is, purely adherent contact (Mesarovic and Fleck 1999). Nonlocal friction was studied in Jelagin and Larsson (2013).

There is a very substantial literature on indentation and the interaction of isolated asperities. The contact between different elastoplastic materials was studied in Eriten et al. (2012); Olsson and Larsson (2016). In addition to the properties of normal contact with and without friction, contact with adhesion plays an important role at small scales especially for noble metals that oxidize less than other metals. This is also the case for wear studies, where surface oxides are removed by wear making the interface more adhesive. Studies on adhesive contact between elastoplastic rough asperities can be found in Olsson and Larsson (2013). Even more important for the understanding of interface physics are studies of tangential motion between elastic or elastoplastic asperities starting with work by Green (1954); Greenwood and Tabor (1955) on the deformation of asperities in plasticine, which was followed by many studies (Cocks 1966; Challen and Oxley 1979; Black et al. 1993), among other numerical studies (such as for example, Tangena and Wijnhoven 1985; Faulkner and Arnell 2000; Kogut and Etsion 2003b; Jackson et al. 2007; Eriten et al. 2010; Mulvihill et al. 2011). However, in many studies, asperities are simulated as half-spheres, which reduces the relevance of quantitative results for true roughness; the same remark concerns the use of the Coulomb-type law of friction which, as has already been mentioned several times, is not relevant for contact between asperities and which must be replaced by Tresca friction.

The interest of all studies of asperities or isolated indentors is to be able to feed mesoscopic models that are based on the notion of asperities and their interaction (Yastrebov et al. 2011; Afferrante et al. 2012). In addition, the results obtained for isolated asperities can be used for the construction or validation of

9 The invalidity of Coulomb's law for very high pressure is explained by the fact that the contact area saturates and the maximum resistance also does so accordingly.

phenomenological models (Hulikal et al. 2015). In the study by Yastrebov et al. (2011), numerous large-strain elastoplastic calculations on isolated asperities resulted in constructing a response surface of characteristic asperities found on experimental rough surfaces, which was then used in a multi-asperity model with an elastic but short-range interaction[10]. The scale effect in this type of multi-scale calculation was briefly analyzed in Yastrebov (2019) assuming that the hardness depends on the radius of curvature. However, it must be realized that although the interaction between asperities can be taken into account (Ciavarella et al. 2006; Paggi and Ciavarella 2010; Yastrebov et al. 2011; Yastrebov 2019), these models based on the notion of asperities can predict the evolution of the actual area of contact only under low pressure when the contact areas remain associated with isolated asperities. The consideration of junction of contact areas associated with neighboring asperities cannot be rigorously achieved in these models and remains a very important growth mechanism of the real contact area (Eid and Adams 2007; Greenwood 2007; Yastrebov et al. 2014).

3.5. Application II: rough surface contact

As explained above, the study of contact between isolated asperities has its limitations and cannot be directly used to build mesoscopic models capable of dealing with the problem of contact between rough surfaces for arbitrary loading. This type of problem can therefore be directly addressed by simulating the contact between two deformable rough surfaces or a deformable rough surface and a rigid plane or a rigid rough surface and a deformable half-space. The requirements for tackling this problem are (1) the construction of one or more rough surfaces and (2) the solution of normal, and possibly tangential, contact between these surfaces. As already mentioned, at the discretization scale, the surfaces must be smooth to allow convergence to a solution with mesh refinement. This involves the implementation of a smoothing procedure for real topographic measurements, which is not very difficult because these are often carried out on regular grids. The smoothing can be done by Béziers surfaces (Pietrzak 1997; Yastrebov et al. 2011), NURBS (Laursen 2002), or even by Shanon interpolation[11] (Hyun and Robbins 2007; An et al. 2019). This issue was discussed in detail in Thompson and Thompson (2010).

---

10 There are configuration cases where plasticity is localized near the asperities in contact, and the interaction between asperities can be considered elastic.

11 Here, Shanon interpolation refer to Whittaker–Kotel'nikov–Shannon interpolation (Marks 2012) applicable to limited-band signals that interpolates Fourier series that can be evaluated at all points. This interpolation is applicable to two- and three-dimensional signals. The fact that it uses limited band indeed concurs with the need for small-scale smooth surfaces which is required for the convergence of mechanical computation.

For part (2) simulations, the challenges related to the capability of supercomputers to make this type of computation arises immediately. If we take as a reference mesh the one utilized for modeling the contact between two spherical asperities (Mulvihill et al. 2011) with $\approx 190,000$ tetrahedral and hexahedral elements for two quarters of the spheres, it then implies that for simulating a hundred asperities, it would be necessary to solve a system with a number of degrees of freedom $N_{dof} \approx 3 \times 100 \times 190,000 \times 2 \times 1.5 = 171 \times 10^6$, where the factor 3 takes into account the number of degrees of freedom (DOF) per node, the factor 100 is the number of asperities, the factor 2 is used for simulating the half-spheres of the asperities instead of the quarters, and the factor 1.5 to take into account the coarse mesh of the underlying volume and the spacing between asperities. A solution to the problem associated with so many DOFs seems rather realistic for high-performance computers capable of modern performances and for the level of parallelism of computational codes[12] (Dostál et al. 2019). On the other hand, contact calculations between asperities of such magnitude do not yet exist. Moreover, it should be noted that mesh optimization and remeshing procedures will be very significant to perform this type of calculation.

The history of contact calculations between rough surfaces begins with the first calculations that were made with boundary elements combined with a finite element layer on the surface: the two (Francis 1982, 1983b) and three-dimensional methods (Francis 1983a) called surface finite elements[13]. Also two-dimensional, a similar technique was used for slip analysis for an indentor on a surface with fingerprints (Webster and Sayles 1986). Often, this kind of computation is carried out with the boundary element method or similar which does not require volumetric discretization, but is normally limited to linear, isotropic and homogeneous elastic materials because it is based on the fundamental Boussinesq–Cerutti solution. As examples, we can cite the pioneering research of Lai and Cheng (1985); Seabra and Berthe (1987); Sainsot et al. (1990). One of the first results that took plasticity into account, which was done by saturating the contact pressure to $1.6\sigma_Y$[14], in 3D, was presented in West and Sayles (1987). The importance of solving topographic measurements for addressing contact was highlighted in Myshkin et al. (1998). The study of rough contact between coated solids presents an important problem of tribology, one of the first simulations was presented in Cole and Sayles (1992), other studies can be found in Nogi and Kato (1997); Peng (2001). It should be pointed out that in Nogi and Kato (1997), rough contact between a coated substrate and an indentor was studied in 3D using a spectral technique (see Stanley and Kato 1997 also for spectral methods). In Borri-Brunetto et al. (1998), interesting considerations

12 See: https://www.lnm.mw.tum.de/en/research/research-fields/highperformance-computing.

13 This is probably the first article in which three-dimensional simulations were presented.

14 Strangely, the authors took a value equal to $1.6\sigma_Y$ for hardness which corresponds to the plasticity initiation pressure even though it was already well known that plasticity onset pressure and pressure saturation (hardness) values correspond to the different pressures.

and ideas are presented as well as surface models and boundary element method-based analysis. The entire volume, from which this publication is taken, is of interest for roughness and contact studies. One of the earliest treatments of rough contact with friction was carried out by Kalker et al. (1997). Moreover, it is important to note that most boundary element methods for the simulation of rough contact are based on variational principles formulated by Kalker and Van Randen (1972) and Kalker (1977). A fairly detailed study on elastoplastic contact was carried out in Lee and Ren (1996) using a boundary element method (Ren and Lee 1994) to which pressure saturation was added. Moreover, the comment made by Etsion on this last article and the response of the authors reiterate the important question of the relevance of the study of elastic contact. Indeed, as already demonstrated by Greenwood and Williamson (1966), the plasticity index decreases due to the irreversible plastic deformation that flattens the surface and which, after some time, is deformed following an elastic regime: this is often the case with engineering systems which all operate in cyclic loading. In this light, the study of elastoplastic contact is only relevant for the *running-in* regime in which plastic deformation can take place.

A two- and three-dimensional contact analysis method was developed by Lubrecht and Ioannides (1991) based on conventional boundary elements but endowed with a multi-level multi-integration procedure or *multi-level multi-summation*) (Brandt and Lubrecht 1990) making it possible to significantly reduce the cost of convolution evaluation, moreover the authors use the associated multigrid method for also improving the solver. The applications of these methods can be found in many works (Venner and Lubrecht 1996; Polonsky and Keer 1999; Medina and Dini 2014). It should mentioned that the MLMI method with the *Full Multi-Grid* solver did not converge for sufficiently rough surfaces, and by replacing this solver with a conjugate gradient much more stable and faster convergence was ensured (Polonsky and Keer 1999); the use of the gradient conjugated with the FFT method was presented in Ai and Sawamiphakdi (1999). The couplings of the conjugate gradient with MLMI/MLMS or FFT were compared in Polonsky and Keer (2000). Strangely, Xiaolan Ai was thanked by the authors but his article on this type of coupling (see below) was not cited. In Gao et al. (2000), the authors performed one of the first thermo-mechanical simulations of contact heating at the roughness scale due to localized friction on the contact areas. A review of numerical methods for the treatment of rough contact was done in Sayles (1996). Another study that compared different methods (boundary elements) was retaken in Allwood (2005). The most recent review was carried out by Bemporad and Paggi (2015), where the authors compared several methods: (i) a greedy solver algorithm without stress (conjugate gradient, Cholesky, Gauss–Seidel), for example (Borri-Brunetto et al. 1999); (ii) the restricted conjugate gradient method (Polonsky and Keer 1999); (iii) *alternating direction method of multipliers* (Boyd et al. 2011); and (iv) the nonnegative least squares method (Lawson and Hanson 1995, p. 161). In addition,

the authors stress the importance of the initial estimate of contact (*warm start*) for achieving very fast convergence.

In the scientific landscape of the last 15 years, simulations of rough contact by the FEM have begun to emerge (Hyun et al. 2004; Pei et al. 2005; Hyun and Robbins 2007; Yastrebov et al. 2011; Song et al. 2017; An et al. 2019). This method can be used in particular to address problems of nonlinear and heterogeneous materials. The methods of boundary elements are also still being developed by addressing contact with heterogeneous (Koumi et al. 2015), viscoelastic (Carbone and Putignano 2013; Putignano et al. 2015; van Dokkum and Nicola 2019) and elastoplastic bodies (Nelias et al. 2006; Pérez-Ràfols et al. 2016; Frérot et al. 2019) with adhesion (Carbone and Mangialardi 2008; Dapp and Müser 2015; Pohrt and Popov 2015; Müser et al. 2017; Popov et al. 2017; Rey et al. 2017) and friction (Paggi et al. 2014; Pohrt and Li 2014) also utilizing a remeshing procedure (Putignano et al. 2012). These new algorithms are still built based on the variational principles set up by Kalker (1977). The emergence of models based on vibration damping for a system of surface "atoms" interacting through an elastic operator of boundary elements allowed achieving unbelievably fine discretizations (Campañá and Müser 2006; Prodanov et al. 2014; Müser et al. 2017). In Prodanov et al. (2014), the authors present simulations made on a grid comprising $2^{34} \approx 17.18 \times 10^9$ (!) discretization points. However, this technique is not based on variational principles, in other words, there is no underlying minimization problem.

PURELY GEOMETRIC CONTACT MODEL.– In Pei et al. (2005), the authors demonstrated the inconsistency of the geometric subtraction model between two rough surfaces to determine the actual contact area, which was used in Sayles and Thomas (1978); Majumdar and Bhushan (1991) and Majumdar and Tien (1991), as well as other models based in particular on the notion of fractal. The geometric subtraction model (which is similar to the Winkler substrate model) is not accurate for elastoplastic contact, let alone elastic contact (a good demonstration of this fact can be found in Dapp et al. (2012)). On the other hand, the model based on the redistribution of the plastic volume (Pullen and Williamson 1972; Nayak 1973) makes more sense despite not taking the elastic interaction into account.

2D SIMULATION OF ROUGH CONTACT.– In the Flamant solution (2D), the stress decreases as $1/r$ and the displacement changes as $\ln(r)$ where r is the distance to the point of application of the force, which creates problems for defining the displacement as it diverges to infinity. In Boussinesq's solution (3D), the asymptotes are $1/r^2$ and $1/r$, respectively, for stress and displacement. As a result, the solutions to both problems are quite different. At the geometry level, the peaks that appear as asperities on a profile are not vertexes (true asperities) that may come into contact, the statistic of the two is not the same, although one can be

deduced from the other (Nayak 1971). This has direct consequences on the mechanics of contact between profiles and surfaces. A direct correction of the 2D results for estimating the contact area as $A = \pi/4 \sum_i l_i^2$ where l_i are separate contact lengths, which, for example, were used in the 2D analysis by Mitchell et al. (2013). Despite that it leads to recovering the linear (or quasi-linear) growth of the contact area with the applied pressure, it cannot be considered as a precise solution. In addition, sealing and lubrication problems in mixed mode cannot be addressed in 2D because a single point of contact blocks the flow of a fluid, which therefore requires an artificial correction that is difficult to properly achieve. 2D and 3D computations were compared by Francis (1983a) to determine what is the level of anisotropy at which the 2D model can be representative of a sinusoidal surface. However, although the level of anisotropy required is not very large, it is unlikely that small-scale roughness be very anisotropic. In conclusion, 2D contact (for profiles) cannot be used for estimating the contact of rough surfaces in 3D.

THE MICROSTRUCTURAL ASPECT OF THE CONTACT.– In addition to surface geometry, the underlying microstructure plays an important part in micromechanical contact. We propose here some references (this list is largely incomprehensive) where this aspect is taken into account in the analysis of contact problems. One of the first microstructural models for *fretting fatigue* for studying microstructure on a regular 2D grid was introduced in Goh et al. (2003). More realistic and 3D microstructures for the same problem were studied in Dick and Cailletaud (2006); Dick et al. (2008). This work was followed by many others (McCarthy et al. 2014; Nigro et al. 2014; Lindroos et al. 2015; Tkalich et al. 2017; Lindroos et al. 2018). Crystal plasticity with the size effect (gradient plasticity) was taken into account in Ashton et al. (2018), which was motivated by observing and modeling the relationship between grain size and *fretting fatigue* crack onset (Ashton et al. 2017). Studies including microstructure as well as roughness are extremely rare (see Durand 2012).

3.6. Conclusion

Great progress has been made in the numerical simulation of microscopic contact with finite element and boundary element methods. However, a few shortcomings that should be addressed can be identified:

– Most studies of contact between asperities employ the Amontons–Coulomb law of friction which is not suitable for small scale. In the future, it would therefore be interesting to redo all of the studies using Tresca's law, which is more relevant for small-scale roughness.

– Another avenue for the future should be to study elastic and elastoplastic contact between *two* rough surfaces. It would be particularly important to better understand

the transition between adhesion and slip that will make the link between static friction and roughness and material parameters. Taking into account the microstructure with its anisotropy and crystal plasticity will be important to draw quantitative results. In addition, it would be interesting to study the viscoelastic behavior that will allow quantifying the state of contact according to time and velocity (for low velocities), which will then make it possible to study dynamic friction. Furthermore, the viscoelastic effect will allow for better understanding the sliding (or flow) of glaciers on the rocky bed as well as accurately formulating the laws of friction that govern it.

– For higher speeds, the viscous effects will no longer be sufficient to understand small-scale frictional sliding. Since friction dissipation is highly localized, the heat produced is such that locally a fusion of the material occurs. Taking this phenomenon into account in highly coupled thermo-mechanical simulation will enable our understanding of this complex phenomenon to be improved.

– Much progress has been made on the simulation of fluid/solid interaction in the contact interface (Lubrecht and Venner 1999; Sahlin et al. 2010; Dapp et al. 2012; Pérez-Ràfols et al. 2016; Stupkiewicz et al. 2016; Temizer et Stupkiewicz 2016; Shvarts and Yastrebov 2018a, 2018b; Ager et al. 2019; Alp çakal et al. 2019; Shvarts 2019; Vlădescu et al. 2019). On the other hand, the strongly coupled finite element model that will allow roughness-scale lubrication in mixed regime to be simulated is still missing (Vakis et al. 2018).

3.7. References

Abramian, B., Arutiunian, N.K., Babloian, A. (1966). On symmetric pressure of a circular stamp on an elastic half-space in the presence of adhesion. *Journal of Applied Mathematics and Mechanics*, 30(1), 173–179.

Adams, G.G. (1995). Self-excited oscillations of two elastic half-spaces sliding with a constant coefficient of friction. *Journal of Applied Mechanics*, 62(4), 867–872.

Adams, G.G. (2000). Radiation of body waves induced by the sliding of an elastic half-space against a rigid surface. *Journal of Applied Mechanics*, 67(1), 1–5.

Adler, R.J. and Taylor, J.E. (2009). *Random Fields and Geometry*. Springer, New York.

Afferrante, L., Carbone, G., Demelio, G. (2012). Interacting and coalescing hertzian asperities: A new multiasperity contact model. *Wear*, 278, 28–33.

Ager, C., Schott, B., Vuong, A.-T., Popp, A., Wall, W.A. (2019). A consistent approach for fluid-structure-contact interaction based on a porous flow model for rough surface contact. *International Journal for Numerical Methods in Engineering*, 119(13), 1345–1378.

Ai, X. and Sawamiphakdi, K. (1999). Solving elastic contact between rough surfaces as an unconstrained strain energy minimization by using CGM and FFT techniques. *Journal of Tribology*, 121(4), 639–647.

Akula, B.R. (2019). Extended mortar method for contact and mesh-tying applications. PhD Thesis, PSL Research University, MINES ParisTech, Paris.

Akula, B.R., Vignollet, J., Yastrebov, V.A. (2019). Mortex method for contact along real and embedded surfaces: Coupling X-FEM with the mortar method. *arXiv:1902.04000*, 60440597.

Alart, P. (1997). Méthode de Newton généralisée en mécanique du contact. *Journal de mathématiques pures et appliqués*, 76, 83–108.

Alart, P. and Curnier, A. (1991). A mixed formulation for frictional contact problems prone to newton like solution methods. *Computer Methods in Applied Mechanics and Engineering*, 92(3), 353–375.

Allwood, J. (2005). Survey and performance assessment of solution methods for elastic rough contact problems. *Journal of Tribology*, 127(1), 10–23.

Altenbach, H., Maugin, G.A., Erofeev, V. (2011). *Mechanics of Generalized Continua*. Springer, Berlin, Heidelberg.

An, B., Wang, X., Xu, Y., Jackson, R.L. (2019). Deterministic elastic-plastic modelling of rough surface contact including spectral interpolation and comparison to theoretical model. *Tribology International*, 135, 246–258.

Andersson, T. (1981). The boundary element method applied to two-dimensional contact problems with friction. In *Boundary Element Methods: Proceedings of the Third International Seminar*, *Irvine, California, July 1981*, Brebia, C.A. (ed.). Springer, Berlin, Heidelberg, 239–258.

Andersson, P. and Kropp, W. (2008). Time domain contact model for tyre/road interaction including nonlinear contact stiffness due to small-scale roughness. *Journal of Sound and Vibration*, 318(1/2), 296–312.

Andrews, D.J. and Ben-Zion, Y. (1997). Wrinkle-like slip pulse on a fault between different material. *Journal of Geophysical Research: Solid Earth*, 102(B1), 553–571.

Archard, J. and Hirst, W. (1956). The wear of metals under unlubricated conditions. *Proc. R. Soc. Lond. A*, 236(1206), 397–410.

Ashton, P., Harte, A.M., Leen, S.B. (2017). Statistical grain size effects in fretting crack initiation. *Tribology International*, 108, 75–86.

Ashton, P., Harte, A., Leen, S. (2018). A strain-gradient, crystal plasticity model for microstructure-sensitive fretting crack initiation in ferritic-pearlitic steel for flexible marine risers. *International Journal of Fatigue*, 111, 81–92.

Autumn, K. (2007). Gecko adhesion: Structure, function, and applications. *Mrs Bulletin*, 32(6), 473–478.

Ballard, P. (1999). A counter-example to uniqueness in quasi-static elastic contact problems with small friction. *International Journal of Engineering Science*, 37(2), 163–178.

Ballard, P. (2016). Steady sliding frictional contact problem for a 2D elastic half-space with a discontinuous friction coefficient and related stress singularities. *Journal of the Mechanics and Physics of Solids*, 97, 225–259.

Ballard, P. and Basseville, S. (2005). Existence and uniqueness for dynamical unilateral contact with coulomb friction: A model problem. *ESAIM: Mathematical Modelling and Numerical Analysis*, 39(1), 59–77.

Barras, F., Kammer, D.S., Geubelle, P.H., Molinari, J.-F. (2014). A study of frictional contact in dynamic fracture along bimaterial interfaces. *International Journal of Fracture*, 189(2), 149–162.

Basseville, S. and Cailletaud, G. (2015). An evaluation of the competition between wear and crack initiation in fretting conditions for Ti–6Al–4V alloy. *Wear*, 328, 443–455.

Basseville, S., Niass, M., Missoum-Benziane, D., Leroux, J., Cailletaud, G. (2019). Effect of fretting wear on crack initiation for cylinder-plate and punch-plane tests. *Wear*, 420, 133–148.

Batailly, A., Magnain, B., Chevaugeon, N. (2013). A comparative study between two smoothing strategies for the simulation of contact with large sliding. *Computational Mechanics*, 51(5), 581–601.

Bathe, K.-J. (1996). *Finite Element Procedures*. Prentice Hall, Upper Saddle River, NJ.

Belgacem, F.B., Hild, P., Laborde, P. (1999). Extension of the mortar finite element method to a variational inequality modeling unilateral contact. *Mathematical Models and Methods in Applied Sciences*, 9(2), 287–303.

Belytschko, T., Daniel, W., Ventura, G. (2002). A monolithic smoothing-gap algorithm for contact-impact based on the signed distance function. *International Journal for Numerical Methods in Engineering*, 55(1), 101–125.

Bemporad, A. and Paggi, M. (2015). Optimization algorithms for the solution of the frictionless normal contact between rough surfaces. *International Journal of Solids and Structures*, 69, 94–105.

Bertsekas, D., Nedic, A., Ozdaglar, A. (2003). *Convex Analysis and Optimization*. Athena Scientific, Belmont.

Black, A., Kopalinsky, E., Oxley, P. (1993). Asperity deformation models for explaining the mechanisms involved in metallic sliding friction and wear – A review. *Proceedings of the Institution of Mechanical Engineers, Part C: Journal of Mechanical Engineering Science*, 207(5), 335–353.

Borri-Brunetto, M., Carpinteri, A., Chiaia, B. (1998). Lacunarity of the contact domain between elastic bodies with rough boundaries. In *PROBAMAT – 21st Century: Probabilities and Materials*, Frantziskonis, G.N. (ed.). Springer, Dordrecht. doi: 10.1007/978-94-011-5216-7_3.

Borri-Brunetto, M., Carpinteri, A., Chiaia, B. (1999). Scaling phenomena due to fractal contact in concrete and rock fractures. In *Fracture Scaling*, Bažant, Z.P. and Rajapakse, Y.D.S. (eds). Springer, Dordrecht. doi: 10.1007/978-94-011-4659-3_12.

Bowden, F.P. and Tabor, D. (1986). *The Friction and Lubrication of Solids*. Oxford University Press, Oxford.

Boyd, S., Parikh, N., Chu, E., Peleato, B., Eckstein, J. (2011). Distributed optimization and statistical learning via the alternating direction method of multipliers. *Foundations and Trends in Machine Learning*, 3(1), 1–122.

Brandt, A. and Lubrecht, A. (1990). Multilevel matrix multiplication and fast solution of integral equations. *Journal of Computational Physics*, 90(2), 348–370.

Brener, E.A., Weikamp, M., Spatschek, R., Bar-Sinai, Y., Bouchbinder, E. (2016). Dynamic instabilities of frictional sliding at a bimaterial interface. *Journal of the Mechanics and Physics of Solids*, 89, 149–173.

Brizmer, V., Kligerman, Y., Etsion, I. (2007). Elastic-plastic spherical contact under combined normal and tangential loading in full stick. *Tribology Letters*, 25(1), 61–70.

Bui, H.D. and Oueslati, A. (2010). On the stick-slip waves under unilateral contact and coulomb friction. *Annals of Solid and Structural Mechanics*, 1(3/4), 159–172.

Bussetta, P., Marceau, D., Ponthot, J.-P. (2012). The adapted augmented Lagrangian method: A new method for the resolution of the mechanical frictional contact problem. *Computational Mechanics*, 49(2), 259–275.

Çakal, B.A., Temizer, I., Terada, K., Kato, J. (2019). Microscopic design and optimization of hydrodynamically lubricated dissipative interfaces. *International Journal for Numerical Methods in Engineering*, 120(2), 153–178.

Campañá, C. and Müser, M.H. (2006). Practical Green's function approach to the simulation of elastic semi-infinite solids. *Physical Review B*, 74(7), 075420.

Campañá, C., Persson, B., Müser, M. (2011). Transverse and normal interfacial stiffness of solids with randomly rough surfaces. *Journal of Physics: Condensed Matter*, 23(8), 085001.

Carbone, G. and Mangialardi, L. (2008). Analysis of the adhesive contact of confined layers by using a Green's function approach. *Journal of the Mechanics and Physics of Solids*, 56(2), 684–706.

Carbone, G. and Putignano, C. (2013). A novel methodology to predict sliding and rolling friction of viscoelastic materials: Theory and experiments. *Journal of the Mechanics and Physics of Solids*, 61(8), 1822–1834.

Casals, O. and Forest, S. (2009). Finite element crystal plasticity analysis of spherical indentation in bulk single crystals and coatings. *Computational Materials Science*, 45(3), 774–782.

Cattaneo, C. (1938). Sul contatto de due corpi elastici: Distribuzione locale deglisforzi. *Rendiconti dell'Accademia nazionale dei Lincei*, 27, 342–349.

Challen, J. and Oxley, P. (1979). An explanation of the different regimes of friction and wear using asperity deformation models. *Wear*, 53(2), 229–243.

Chamoret, D., Saillard, P., Rassineux, A., Bergheau, J.-M. (2004). New smoothing procedures in contact mechanics. *Journal of Computational and Applied Mathematics*, 168, 107–116.

Chang, H.-J., Fivel, M., Rodney, D., Verdier, M. (2010). Multiscale modelling of indentation in fcc metals: From atomic to continuum. *Comptes Rendus Physique*, 11(3/4), 285–292.

Chaudhary, A.B. and Bathe, K.-J. (1986). A solution method for static and dynamic analysis of three-dimensional contact problems with friction. *Computers & Structures*, 24(6), 855–873.

Chen, X. and Hisada, T. (2006). Development of a finite element contact analysis algorithm to pass the patch test. *JSME International Journal Series A Solid Mechanics and Material Engineering*, 49(4), 483–491.

Chen, W.W. and Wang, Q.J. (2008). A numerical model for the point contact of dissimilar materials considering tangential tractions. *Mechanics of Materials*, 40(11), 936–948.

Chouly, F. and Hild, P. (2013). A nitsche-based method for unilateral contact problems: Numerical analysis. *SIAM Journal on Numerical Analysis*, 51(2), 1295–1307.

Chouly, F., Hild, P., Renard, Y. (2015). Symmetric and non-symmetric variants of Nitsche's method for contact problems in elasticity: Theory and numerical experiments. *Mathematics of Computation*, 84(293), 1089–1112.

Christensen, P., Klarbring, A., Pang, J.-S., Strömberg, N. (1998). Formulation and comparison of algorithms for frictional contact problems. *International Journal for Numerical Methods in Engineering*, 42(1), 145–173.

Ciavarella, M., Delfine, V., Demelio, G. (2006). A "re-vitalized" Greenwood and Williamson model of elastic contact between fractal surfaces. *Journal of the Mechanics and Physics of Solids*, 54(12), 2569–2591.

Cochard, A. and Rice, J. (2000). Fault rupture between dissimilar materials: Ill-posedness, regularization, and slip-pulse response. *Journal of Geophysical Research: Solid Earth*, 105(B11), 25891–25907.

Cocks, M. (1966). Shearing of junctions between metal surfaces. *Wear*, 9(4), 320–328.

Coker, D., Lykotrafitis, G., Needleman, A., Rosakis, A. (2005). Frictional sliding modes along an interface between identical elastic plates subject to shear impact loading. *Journal of the Mechanics and Physics of Solids*, 53(4), 884–922.

Cole, S. and Sayles, R. (1992). A numerical model for the contact of layered elastic bodies with real rough surfaces. *Journal of Tribology*, 114(2), 334–340.

Cooper, M., Mikic, B., Yovanovich, M. (1969). Thermal contact conductance. *International Journal of Heat and Mass Transfer*, 12(3), 279–300.

Costa, H. and Hutchings, I. (2007). Hydrodynamic lubrication of textured steel surfaces under reciprocating sliding conditions. *Tribology International*, 40(8), 1227–1238.

Crisfield, M. (2000). Re-visiting the contact patch test. *International Journal for Numerical Methods in Engineering*, 48(3), 435–449.

Curnier, A. (1984). A theory of friction. *International Journal of Solids and Structures*, 20, 637–647.

Dapp, W.B. and Müser, M.H. (2015). Contact mechanics of and reynolds flow through saddle points: On the coalescence of contact patches and the leakage rate through near-critical constrictions. *EPL (Europhysics Letters)*, 109(4), 44001.

Dapp, W.B. and Müser, M.H. (2016). Fluid leakage near the percolation threshold. *Scientific Reports*, 6, 19513. doi: 10.1038/srep19513.

Dapp, W.B., Lücke, A., Persson, B.N., Müser, M.H. (2012). Self-affine elastic contacts: Percolation and leakage. *Physical Review Letters*, 108(24), 244301.

De Lorenzis, L., Temizer, I., Wriggers, P., Zavarise, G. (2011). A large deformation frictional contact formulation using NURBS-based isogeometric analysis. *International Journal for Numerical Methods in Engineering*, 87(13), 1278–1300.

De Lorenzis, L., Wriggers, P., Hughes, T.J. (2014). Isogeometric contact: A review. *GAMM-Mitteilungen*, 37(1), 85–123.

Dick, T. and Cailletaud, G. (2006). Fretting modelling with a crystal plasticity model of Ti6Al4V. *Computational Materials Science*, 38(1), 113–125.

Dick, T., Basseville, S., Cailletaud, G. (2008). Fatigue modelling in fretting contact with a crystal plasticity model. *Computational Materials Science*, 43(1), 36–42.

Dieterich, J.H. (1992). Earthquake nucleation on faults with rate-and state-dependent strength. *Tectonophysics*, 211(1/4), 115–134.

Dieterich, J.H. and Kilgore, B.D. (1994). Direct observation of frictional contacts: New insights for state-dependent properties. *Pure and Applied Geophysics*, 143(1/3), 283–302.

van Dokkum, J.S. and Nicola, L. (2019). Green's function molecular dynamics including viscoelasticity. *Modelling and Simulation in Materials Science and Engineering*, 27, 075006. doi: 10.1088/1361-651X/ab3031.

Dostál, Z., Kozubek, T., Sadowská, M., Vondrák, V. (2016). *Scalable Algorithms for Contact Problems*. Springer, Cham.

Dostál, Z., Vlach, O., Brzobohatá, T. (2019). Scalable TFETI based algorithm with adaptive augmentation for contact problems with variationally consistent discretization of contact conditions. *Finite Elements in Analysis and Design*, 156, 34–43.

Durand, J. (2012). Approche multi-échelles des problèmes de contact et d'étanchéité. PhD Thesis, MINES ParisTech, Paris [Online]. Available at: https://pastel.archives-ouvertes.fr/pastel-00820173.

Duvaut, G. and Lions, J.L. (1972). *Les inéquations en mécanique et en physique*. Dunod, Paris.

Eid, H. and Adams, G.G. (2007). An elastic-plastic finite element analysis of interacting asperities in contact with a rigid flat. *Journal of Physics D: Applied Physics*, 40(23), 7432.

El-Abbasi, N. and Bathe, K.-J. (2001). Stability and patch test performance of contact discretizations and a new solution algorithm. *Computers & Structures*, 79(16), 1473–1486.

Elkilani, Y.S. (2003). A hybrid elasticity and finite element method for three-dimensional contact problems with friction. PhD Thesis, University of Cincinnati, Cincinnati.

Eringen, A.C. (1999). *Microcontinuum Field Theories: I. Foundations and Solids*. Springer, New York.

Eriten, M., Polycarpou, A., Bergman, L. (2010). Physics-based modeling for partial slip behavior of spherical contacts. *International Journal of Solids and Structures*, 47(18/19), 2554–2567.

Eriten, M., Petlicki, D., Polycarpou, A., Bergman, L. (2012). Influence of friction and adhesion on the onset of plasticity during normal loading of spherical contacts. *Mechanics of Materials*, 48, 26–42.

Etsion, I., Kligerman, Y., Kadin, Y. (2005). Unloading of an elastic-plastic loaded spherical contact. *International Journal of Solids and Structures*, 42(13), 3716–3729.

Farah, P., Gitterle, M., Wall, W.A., Popp, A. (2016). Computational wear and contact modeling for fretting analysis with isogeometric dual mortar methods. *Key Engineering Materials*, 681, 1–18. doi: 10.4028/www.scientific.net/kem.681.1.

Faulkner, A. and Arnell, R. (2000). The development of a finite element model to simulate the sliding interaction between two, three-dimensional, elastoplastic, hemispherical asperities. *Wear*, 242(1/2), 114–122.

Feng, G. and Nix, W.D. (2004). Indentation size effect in MgO. *Scripta Materialia*, 51(6), 599–603.

Fischer-Cripps, A.C. (2011). Nanoindentation testing. In *Nanoindentation*. Springer, New York.

Fivel, M., Robertson, C., Canova, G., Boulanger, L. (1998). Three-dimensional modeling of indent-induced plastic zone at a mesoscale. *Acta Materialia*, 46(17), 6183–6194.

Forest, S. (1998). Mechanics of generalized continua: Construction by homogenizaton. *Le journal de physique IV*, 8(PR4), Pr4-39–Pr4-48.

Francis, H. (1982). A finite surface element model for plane-strain elastic contact. *Wear*, 76(2), 221–245.

Francis, H. (1983a). The accuracy of plane strain models for the elastic contact of three-dimensional rough surfaces. *Wear*, 85(2), 239–256.

Francis, H. (1983b). A finite surface element model for two concentric nearly circular rings in partial contact. *Computers & Structures*, 17(2), 169–176.

Frérot, L., Bonnet, M., Molinari, J.-F., Anciaux, G. (2019). A Fourier-accelerated volume integral method for elastoplastic contact. *Computer Methods in Applied Mechanics and Engineering*, 351, 951–976.

Gallego, L., Nelias, D., Deyber, S. (2010). A fast and efficient contact algorithm for fretting problems applied to fretting modes i, ii and iii. *Wear*, 268(1/2), 208–222.

Gao, J., Lee, S.C., Ai, X., Nixon, H. (2000). An FFT-based transient flash temperature model for general three-dimensional rough surface contacts. *Transactions – ASME Journal of Tribology*, 122(3), 519–523.

Gao, Y., Larson, B.C., Lee, J., Nicola, L., Tischler, J., Pharr, G.M. (2015). Lattice rotation patterns and strain gradient effects in face-centered-cubic single crystals under spherical indentation. *Journal of Applied Mechanics*, 82(6), 061007.

Gerde, E. and Marder, M. (2001). Friction and fracture. *Nature*, 413(6853), 285.

Gitterle, M., Popp, A., Gee, M.W., Wall, W.A. (2010). Finite deformation frictional mortar contact using a semi-smooth Newton method with consistent linearization. *International Journal for Numerical Methods in Engineering*, 84(5), 543–571.

Gnecco, E. and Meyer, E. (2015). *Fundamentals of Friction and Wear on the Nanoscale*. Springer, Cham.

Gnecco, E., Bennewitz, R., Gyalog, T., Loppacher, C., Bammerlin, M., Meyer, E., Güntherodt, H.-J. (2000). Velocity dependence of atomic friction. *Physical Review Letters*, 84(6), 1172.

Goh, C.-H., Neu, R.W., McDowell, D.L. (2003). Crystallographic plasticity in fretting of TI–6AL–4V. *International Journal of Plasticity*, 19(10), 1627–1650.

Goodman, L. and Hamilton, G. (1966). The stress field created by a circular sliding contact. *ASME J. Appl. Mech.*, 33(2), 371–376.

Green, A. (1954). The plastic yielding of metal junctions due to combined shear and pressure. *Journal of the Mechanics and Physics of Solids*, 2(3), 197–211.

Greenwood, J.A. (1966). Constriction resistance and the real area of contact. *British Journal of Applied Physics*, 17(12), 1621.

Greenwood, J.A. (2007). A note on Nayak's third paper. *Wear*, 262(1/2), 225–227.

Greenwood, J.A. and Tabor, D. (1955). Deformation properties of friction junctions. *Proceedings of the Physical Society. Section B*, 68(9), 609.

Greenwood, J.A. and Tripp, J.H. (1967). The elastic contact of rough spheres. *Journal of Applied Mechanics*, 34(1), 153–159.

Greenwood, J.A. and Williamson, J.B.P. (1966). Contact of nominally flat surfaces. *P. Roy. Soc. Lond. A Mat.*, 295, 300–319.

Guyot, N., Kosior, F., Maurice, G. (2000). Coupling of finite elements and boundary elements methods for study of the frictional contact problem. *Computer Methods in Applied Mechanics and Engineering*, 181(1/3), 147–159.

Gwinner, J. (2013). hp-FEM convergence for unilateral contact problems with Tresca friction in plane linear elastostatics. *Journal of Computational and Applied Mathematics*, 254, 175–184.

Hamilton, G. (1983). Explicit equations for the stresses beneath a sliding spherical contact. *Proceedings of the Institution of Mechanical Engineers, Part C: Journal of Mechanical Engineering Science*, 197(1), 53–59.

Harrison, E. (1990). Olbers' paradox in recent times. In *Modern Cosmology in Retrospect*, Bertotti, B., Balbinot, R., Bergia, S., Messina, A. (eds). Cambridge University Press, Cambridge.

Hartmann, S., Oliver, J., Cante, J., Weyler, R., Hernández, J. (2009). A contact domain method for large deformation frictional contact problems. Part 2: Numerical aspects. *Computer Methods in Applied Mechanics and Engineering*, 198, 2607–2631.

Heaton, T.H. (1990). Evidence for and implications of self-healing pulses of slip in earthquake rupture. *Physics of the Earth and Planetary Interiors*, 64(1), 1–20.

Heegaard, J.-H. and Curnier, A. (1996). Geometric properties of 2D and 3D unilateral large slip contact operators. *Computer Methods in Applied Mechanics and Engineering*, 131, 263–286.

Heege, A. and Alart, P. (1996). A frictional contact element for strongly curved contact problems. *International Journal for Numerical Methods in Engineering*, 39(1), 165–184.

Herrmann, K. (ed.) (2011). *Hardness Testing: Principles and Applications*. ASM International, Almere.

Hertz, H. (1881). On the contact of elastic solids. *Z. Reine Angew. Mathematik*, 92, 156–171.

Hetenyi, M. and McDonald, P. (1958). Contact stresses under combined pressure and twist. *Journal of Applied Mechanics*, 25, 396–401.

Hill, R., Storåkers, B., Zdunek, A. (1989). A theoretical study of the brinell hardness test. *Proc. R. Soc. Lond. A*, 423(1865), 301–330.

Hills, D. and Sackfield, A. (1987). The stress field induced by normal contact between dissimilar spheres. *Journal of Applied Mechanics*, 54(1), 8–14.

Hol, J., Alfaro, M.C., de Rooij, M.B., Meinders, T. (2012). Advanced friction modeling for sheet metal forming. *Wear*, 286, 66–78.

Hu, Y.Z. and Tonder, K. (1992). Simulation of 3-D random rough surface by 2-D digital filter and fourier analysis. *Int. J. Mach. Tool Manu.*, 32, 83–90.

Hulikal, S., Bhattacharya, K., Lapusta, N. (2015). Collective behavior of viscoelastic asperities as a model for static and kinetic friction. *Journal of the Mechanics and Physics of Solids*, 76, 144–161.

Hyun, S. and Robbins, M.O. (2007). Elastic contact between rough surfaces: Effect of roughness at large and small wavelengths. *Tribology International*, 40(10/12), 1413–1422.

Hyun, S., Pei, L., Molinari, J.F., Robbins, M.O. (2004). Finite-element analysis of contact between elastic self-affine surfaces. *Phys. Rev. E.*, 70(2), 026117.

Jackson, R.L., Duvvuru, R.S., Meghani, H., Mahajan, M. (2007). An analysis of elasto-plastic sliding spherical asperity interaction. *Wear*, 262(1/2), 210–219.

Jelagin, D. and Larsson, P.-L. (2012). On indenter boundary effects at elastic contact. *Journal of Mechanics of Materials and Structures*, 7(2), 165–182.

Jelagin, D. and Larsson, P.-L. (2013). Nonlocal frictional effects at indentation of elastic materials. *Tribology Letters*, 51(3), 397–407.

Jing, H.-S. and Liao, M.-L. (1990). An improved finite element scheme for elastic contact problems with friction. *Computers & Structures*, 35(5), 571–578.

Jinn, J.-T. (1989). Finite element analysis of elastic contact problems with friction. PhD Thesis, Ohio State University, Columbus.

Johnson, K.L. (1985). *Contact Mechanics*. Cambridge University Press, Cambridge.

Johnson, K.L., Greenwood, J., Higginson, J. (1985). The contact of elastic regular wavy surfaces. *Int. J. Mech. Sci.*, 27(6), 383 –396.

Kadin, Y., Kligerman, Y., Etsion, I. (2006). Multiple loading-unloading of an elastic-plastic spherical contact. *International Journal of Solids and Structures*, 43(22/23), 7119–7127.

Kalker, J. (1977). Variational principles of contact elastostatics. *IMA Journal of Applied Mathematics*, 20(2), 199–219.

Kalker, J. and Van Randen, Y. (1972). A minimum principle for frictionless elastic contact with application to non-Hertzian half-space contact problems. *Journal of Engineering Mathematics*, 6(2), 193–206.

Kalker, J., Dekking, F., Vollebregt, E. (1997). Simulation of rough, elastic contacts. *Journal of Applied Mechanics*, 64(2), 361–368.

Kammer, D.S., Yastrebov, V., Anciaux, G., Molinari, J. (2014). The existence of a critical length scale in regularised friction. *Journal of the Mechanics and Physics of Solids*, 63, 40–50.

Kammer, D.S., Radiguet, M., Ampuero, J.-P., Molinari, J.-F. (2015). Linear elastic fracture mechanics predicts the propagation distance of frictional slip. *Tribology Letters*, 57(3), 23.

Kikuchi, N. and Oden, J. (1988). *Contact Problems in Elasticity: A Study of Variational Inequalities and Finite Element Methods*. SIAM, Philadelphia.

Kim, J.H. and Jang, Y.H. (2014). Frictional hertzian contact problems under cyclic loading using static reduction. *International Journal of Solids and Structures*, 51(1), 252–258.

Kim, Y.-C., Gwak, E.-J., Ahn, S.-M., Kang, N.-R., Han, H.N., Jang, J.-I., Kim, J.-Y. (2018). Indentation size effect for spherical nanoindentation on nanoporous gold. *Scripta Materialia*, 143, 10–14.

Kinkaid, N., O'Reilly, O.M., Papadopoulos, P. (2003). Automotive disc brake squeal. *Journal of Sound and Vibration*, 267(1), 105–166.

Klang, M. (1979). On interior contact under friction between cylindrical elastic bodies. PhD Thesis, Linköping University, Linköping.

Klarbring, A. (1990a). Derivation and analysis of rate boundary-value problems of frictional contact. *European Journal of Mechanics. A Solids*, 9(1), 53–85.

Klarbring, A. (1990b). Examples of non-uniqueness and non-existence of solutions to quasistatic contact problems with friction. *Archive of Applied Mechanics*, 60(8), 529–541.

Klarbring, A. and Björkman, G. (1992). Solution of large displacement contact problems with friction using Newton's method for generalized equations. *International Journal for Numerical Methods in Engineering*, 34(1), 249–269.

Kogut, L. and Etsion, I. (2002). Elastic-plastic contact analysis of a sphere and a rigid flat. *Journal of Applied Mechanics*, 69(5), 657–662.

Kogut, L. and Etsion, I. (2003a). A finite element based elastic-plastic model for the contact of rough surfaces. *Tribology Transactions*, 46(3), 383–390.

Kogut, L. and Etsion, I. (2003b). A semi-analytical solution for the sliding inception of a spherical contact. *Journal of Tribology*, 125(3), 499–506.

Komvopoulos, K. (1989). Elastic-plastic finite element analysis of indented layered media. *Journal of Tribology*, 111(3), 430–439.

Konyukhov, A. and Schweizerhof, K. (2012). *Computational Contact Mechanics: Geometrically Exact Theory for Arbitrary Shaped Bodies*. Springer, Berlin, Heidelberg.

Korelc, J. (1997). Automatic generation of finite-element code by simultaneous optimization of expressions. *Theoretical Computer Science*, 187(1/2), 231–248.

Kosior, F., Guyot, N., Maurice, G. (1999). Analysis of frictional contact problem using boundary element method and domain decomposition method. *International Journal for Numerical Methods in Engineering*, 46(1), 65–82.

Koumi, K.E., Chaise, T., Nelias, D. (2015). Rolling contact of a rigid sphere/sliding of a spherical indenter upon a viscoelastic half-space containing an ellipsoidal inhomogeneity. *Journal of the Mechanics and Physics of Solids*, 80, 1–25.

Kral, E., Komvopoulos, K., Bogy, D. (1993). Elastic-plastic finite element analysis of repeated indentation of a half-space by a rigid sphere. *Journal of Applied Mechanics*, 60(4), 829–841.

Kravchuk, A. (2008). The solution of three-dimensional friction contact problems. *Journal of Applied Mathematics and Mechanics*, 72(3), 338–346.

Krim, J. (1996). Friction at the atomic scale. *Scientific American*, 275(4), 74–80.

Krim, J. (2002). Surface science and the atomic-scale origins of friction: What once was old is new again. *Surface Science*, 500(1/3), 741–758.

Kwak, B.M. and Lee, S.S. (1988). A complementarity problem formulation for two-dimensional frictional contact problems. *Computers & Structures*, 28(4), 469–480.

Lai, W. and Cheng, H. (1985). Computer simulation of elastic rough contacts. *ASLE Transactions*, 28(2), 172–180.

Laursen, T. (2002). *Computational Contact and Impact Mechanics: Fundamentals of Modeling Interfacial Phenomena in Nonlinear Finite Element Analysis*. Springer, Berlin, Heidelberg.

Laursen, T. and Simo, J. (1993). A continuum-based finite element formulation for the implicit solution of multibody, large deformation-frictional contact problems. *International Journal for Numerical Methods in Engineering*, 36(20), 3451–3485.

Lawson, C.L. and Hanson, R.J. (1995). *Solving Least Squares Problems*. SIAM, Philadelphia.

Lee, S.-S. (1994). A computational method for frictional contact problem using finite element method. *International Journal for Numerical Methods in Engineering*, 37(2), 217–228.

Lee, S.C. and Ren, N. (1996). Behavior of elastic-plastic rough surface contacts as affected by surface topography, load, and material hardness. *Tribology Transactions*, 39(1), 67–74.

Lekhnitskii, S. (1981). *Theory of Elasticity of an Anisotropic Elastic Body*, 2nd edition. Mir Publishers, Moscow.

Lengiewicz, J. and Stupkiewicz, S. (2013). Efficient model of evolution of wear in quasi-steady-state sliding contacts. *Wear*, 303(1/2), 611–621.

Lengiewicz, J., Korelc, J., Stupkiewicz, S. (2011). Automation of finite element formulations for large deformation contact problems. *International Journal for Numerical Methods in Engineering*, 85(10), 1252–1279.

Lewandowski, M. and Stupkiewicz, S. (2018). Size effects in wedge indentation predicted by a gradient-enhanced crystal-plasticity model. *International Journal of Plasticity*, 109, 54–78.

Li, J. and Berger, E. (2003). A semi-analytical approach to three-dimensional normal contact problems with friction. *Computational Mechanics*, 30(4), 310–322.

Lindroos, M., Ratia, V., Apostol, M., Valtonen, K., Laukkanen, A., Molnar, W., Holmberg, K., Kuokkala, V.-T. (2015). The effect of impact conditions on the wear and deformation behavior of wear resistant steels. *Wear*, 328, 197–205.

Lindroos, M., Laukkanen, A., Cailletaud, G., Kuokkala, V.-T. (2018). Microstructure based modeling of the strain rate history effect in wear resistant hadfield steels. *Wear*, 396, 56–66.

Lubrecht, A. and Ioannides, E. (1991). A fast solution of the dry contact problem and the associated sub-surface stress field, using multilevel techniques. *Journal of Tribology*, 113(1), 128–133.

Lubrecht, A. and Venner, C.H. (1999). Elastohydrodynamic lubrication of rough surfaces. *Proceedings of the Institution of Mechanical Engineers, Part J: Journal of Engineering Tribology*, 213(5), 397–404.

Ma, X., De Rooij, M., Schipper, D. (2010). A load dependent friction model for fully plastic contact conditions. *Wear*, 269(11/12), 790–796.

Majumdar, A. and Bhushan, B. (1991). Fractal model of elastic-plastic contact between rough surfaces. *Journal of Tribology*, 113(1), 1–11.

Majumdar, A. and Tien, C. (1990). Fractal characterization and simulation of rough surfaces. *Wear*, 136(2), 313–327.

Majumdar, A. and Tien, C. (1991). Fractal network model for contact conductance. *Journal of Heat Transfer*, 113(3), 516–525.

Mandelbrot, B.B. (1983). *The Fractal Geometry of Nature*. WH Freeman, New York.

Manoylov, A., Bryant, M.J., Evans, H.P. (2013). Dry elasto-plastic contact of nominally flat surfaces. *Tribology International*, 65, 248–258.

Marks, R.J.I. (2012). *Introduction to Shannon Sampling and Interpolation Theory*. Springer, New York.

Martins, J., Guimarães, J., Faria, L. (1995). Dynamic surface solutions in linear elasticity and viscoelasticity with frictional boundary conditions. *Journal of Vibration and Acoustics*, 117(4), 445–451.

Massi, F., Baillet, L., Giannini, O., Sestieri, A. (2007). Brake squeal: Linear and nonlinear numerical approaches. *Mechanical Systems and Signal Processing*, 21(6), 2374–2393.

Mata, M. and Alcala, J. (2004). The role of friction on sharp indentation. *Journal of the Mechanics and Physics of Solids*, 52(1), 145–165.

Maugin, G.A. and Metrikine, A.V. (eds) (2010). *Mechanics of Generalized Continua: One Hundred Years After the Cosserats*. Springer, New York.

McCarthy, O., McGarry, J., Leen, S. (2014). The effect of grain orientation on fretting fatigue plasticity and life prediction. *Tribology International*, 76, 100–115.

Meakin, P. (1998). *Fractals, Scaling and Growth Far from Equilibrium*. Cambridge University Press, Cambridge.

Medina, S. and Dini, D. (2014). A numerical model for the deterministic analysis of adhesive rough contacts down to the nano-scale. *International Journal of Solids and Structures*, 51(14), 2620–2632.

Mesarovic, S.D. and Fleck, N.A. (1999). Spherical indentation of elastic-plastic solids. *Proceedings of the Royal Society of London A: Mathematical, Physical and Engineering Sciences*, 455, 2707–2728.

Michalowski, R. and Mróz, Z. (1978). Associated and non-associated sliding rules in contact friction problems. *Archives of Mechanics*, 30, 259–276.

Mindlin, R. (1949). Compliance of elastic bodies in contact. *J. Appl. Mech., ASME*, 16, 259–268.

Mitchell, E., Fialko, Y., Brown, K. (2013). Temperature dependence of frictional healing of westerly granite: Experimental observations and numerical simulations. *Geochemistry, Geophysics, Geosystems*, 14(3), 567–582.

Mo, Y., Turner, K.T., Szlufarska, I. (2009). Friction laws at the nanoscale. *Nature*, 457(7233), 1116.

Mohammadi, N.K. and Adams, G.G. (2018). Self-excited oscillations of a finite-thickness elastic layer sliding against a rigid surface with a constant coefficient of friction. *Journal of Applied Mechanics*, 85(2), 021005.

Moirot, F., Nguyen, Q.-S., Oueslati, A. (2003). An example of stick-slip and stick-slip-separation waves. *European Journal of Mechanics – A/Solids*, 22(1), 107–118.

Moreau, J.-J. (1966). Fonctionnelles convexes. *Séminaire Jean Leray*, 1966–1967(2), 1–108.

Mossakovskii, V. (1954). The fundamental mixed problem of the theory of elasticity for a half-space with a circular line separating the boundary conditions. *Prikl. Mat. Mekh*, 18(2), 187–196.

Mossakovskii, V. (1963). Compression of elastic bodies under conditions of adhesion (axisymmetric case). *Journal of Applied Mathematics and Mechanics*, 27(3), 630–643.

Mulvihill, D.M., Kartal, M.E., Nowell, D., Hills, D.A. (2011). An elastic-plastic asperity interaction model for sliding friction. *Tribology International*, 44(12), 1679–1694.

Munoz, J. (2008). Modelling unilateral frictionless contact using the null-space method and cubic b-spline interpolation. *Computer Methods in Applied Mechanics and Engineering*, 197(9/12), 979–993.

Müser, M.H., Dapp, W.B., Bugnicourt, R., Sainsot, P., Lesaffre, N., Lubrecht, T.A., Persson, B.N., Harris, K., Bennett, A., Schulze, K. et al. (2017). Meeting the contact-mechanics challenge. *Tribology Letters*, 65(4), 118.

Myshkin, N., Petrokovets, M., Chizhik, S. (1998). Simulation of real contact in tribology. *Tribology International*, 31(1/3), 79–86.

Nayak, P.R. (1971). Random process model of rough surfaces. *J. Lubr. Technol. (ASME)*, 93, 398–407.

Nayak, P.R. (1973). Random process model of rough surfaces in plastic contact. *Wear*, 26(3), 305–333.

Nelias, D., Boucly, V., Brunet, M. (2006). Elastic-plastic contact between rough surfaces: Proposal for a wear or running-in model. *Journal of Tribology*, 128(2), 236–244.

Nigro, C., Sun, L., Meriaux, J., Proudhon, H. (2014). Microstructural simulations of the initiation and propagation of short fretting cracks in a Ti–6al–4v contact. *Tribology International*, 74, 103–109.

Nix, W.D. and Gao, H. (1998). Indentation size effects in crystalline materials: A law for strain gradient plasticity. *Journal of the Mechanics and Physics of Solids*, 46(3), 411–425.

Nogi, T. and Kato, T. (1997). Influence of a hard surface layer on the limit of elastic contact – Part I: Analysis using a real surface model. *Journal of Tribology*, 119(3), 493–500.

Nowell, D., Hills, D., Sackfield, A. (1988). Contact of dissimilar elastic cylinders under normal and tangential loading. *Journal of the Mechanics and Physics of Solids*, 36(1), 59–75.

Oliver, W.C. and Pharr, G.M. (1992). An improved technique for determining hardness and elastic modulus using load and displacement sensing indentation experiments. *Journal of Materials Research*, 7(6), 1564–1583.

Oliver, J., Hartmann, S., Cante, J., Weyler, R., Hernández, J. (2009). A contact domain method for large deformation frictional contact problems. Part 1: Theoretical basis. *Computer Methods in Applied Mechanics and Engineering*, 198, 2591–2606.

Olsson, E. and Larsson, P.-L. (2013). On force-displacement relations at contact between elastic-plastic adhesive bodies. *Journal of the Mechanics and Physics of Solids*, 61(5), 1185–1201.

Olsson, E. and Larsson, P.-L. (2016). A unified model for the contact behaviour between equal and dissimilar elastic-plastic spherical bodies. *International Journal of Solids and Structures*, 81, 23–32.

Özel, T. (2006). The influence of friction models on finite element simulations of machining. *International Journal of Machine Tools and Manufacture*, 46(5), 518–530.

Paggi, M. and Ciavarella, M. (2010). The coefficient of proportionality κ between real contact area and load, with new asperity models. *Wear*, 268(7/8), 1020–1029.

Paggi, M., Pohrt, R., Popov, V.L. (2014). Partial-slip frictional response of rough surfaces. *Scientific Reports*, 4, 5178.

Panagiotopoulos, P. (1975). A nonlinear programming approach to the unilateral contact-, and friction-boundary value problem in the theory of elasticity. *Archive of Applied Mechanics*, 44(6), 421–432.

Pei, L., Hyun, S., Molinari, J.F., Robbins, M.O. (2005). Finite element modeling of elasto-plastic contact between rough surfaces. *J. Mech. Phys. Solids*, 53, 2385–2409.

Peng, W. (2001). Contact mechanics of multilayered rough surfaces in tribology. PhD Thesis, Ohio State University, Columbus.

Pérez-Ràfols, F. and Almqvist, A. (2019). Generating randomly rough surfaces with given height probability distribution and power spectrum. *Tribology International*, 131, 591–604.

Pérez-Ràfols, F., Larsson, R., Almqvist, A. (2016). Modelling of leakage on metal-to-metal seals. *Tribology International*, 94, 421–427.

Pietrzak, G. (1997). Continuum mechanics modelling and augmented Lagrangian formulation of large deformation frictional contact problems. PhD Thesis, École Polytechnique Fédérale de Lausanne, Lausanne.

Pietrzak, G. and Curnier, A. (1999). Large deformation frictional contact mechanics: Continuum formulation and augmented Lagrangian treatment. *Computer Methods in Applied Mechanics and Engineering*, 177(3/4), 351–381.

Plouraboué, F., Geoffroy, S., Prat, M. (2004). Conductances between confined rough walls. *Physics of Fluids*, 16(3), 615–624.

Pohrt, R. and Li, Q. (2014). Complete boundary element formulation for normal and tangential contact problems. *Physical Mesomechanics*, 17(4), 334–340.

Pohrt, R. and Popov, V.L. (2012). Normal contact stiffness of elastic solids with fractal rough surfaces. *Physical Review Letters*, 108(10), 104301.

Pohrt, R. and Popov, V.L. (2015). Adhesive contact simulation of elastic solids using local mesh-dependent detachment criterion in boundary elements method. *Facta Universitatis, Series: Mechanical Engineering*, 13(1), 3–10.

Polonsky, I. and Keer, L.M. (1999). A numerical method for solving rough contact problems based on the multi-level multi-summation and conjugate gradient techniques. *Wear*, 231(2), 206–219.

Polonsky, I. and Keer, L.M. (2000). Fast methods for solving rough contact problems: A comparative study. *Journal of Tribology*, 122(1), 36–41.

Popov, V.L. and Pohrt, R., Li, Q. (2017). Strength of adhesive contacts: Influence of contact geometry and material gradients. *Friction*, 5(3), 308–325.

Popp, A. (2012). Mortar methods for computational contact mechanics and general interface problems. PhD Thesis, Technische Universität München, Munich.

Popp, A., Gitterle, M., Gee, M.W., Wall, W.A. (2010). A dual mortar approach for 3D finite deformation contact with consistent linearization. *International Journal for Numerical Methods in Engineering*, 83(11), 1428–1465.

Prakash, V. (1995). A pressure-shear plate impact experiment for investigating transient friction. *Experimental Mechanics*, 35(4), 329–336.

Prakash, V. and Clifton, R. (1993). Time resolved dynamic friction measurements in pressure-shear. In *Experimental Techniques in the Dynamics of Deformable Solids*, Ramesh, K.T. (ed.). ASME, New York.

Prodanov, N., Dapp, W.B., Müser, M.H. (2014). On the contact area and mean gap of rough, elastic contacts: Dimensional analysis, numerical corrections, and reference data. *Tribology Letters*, 53(2), 433–448.

Pullen, J. and Williamson, J. (1972). On the plastic contact of rough surfaces. *Proceedings of the Royal Society of London. A. Mathematical and Physical Sciences*, 327(1569), 159–173.

Puso, M.A. and Laursen, T.A. (2002). A 3D contact smoothing method using Gregory patches. *International Journal for Numerical Methods in Engineering*, 54(8), 1161–1194.

Puso, M.A. and Laursen, T.A. (2004). A mortar segment-to-segment contact method for large deformation solid mechanics. *Computer Methods in Applied Mechanics and Engineering*, 193(6/8), 601–629.

Puso, M.A., Laursen, T., Solberg, J. (2008). A segment-to-segment mortar contact method for quadratic elements and large deformations. *Computer Methods in Applied Mechanics and Engineering*, 197(6/8), 555–566.

Putignano, C., Afferrante, L., Carbone, G., Demelio, G. (2012). A new efficient numerical method for contact mechanics of rough surfaces. *Int. J. Solids Struct.*, 49(2), 338–343.

Putignano, C., Carbone, G., Dini, D. (2015). Mechanics of rough contacts in elastic and viscoelastic thin layers. *International Journal of Solids and Structures*, 69, 507–517.

Qiu, X., Huang, Y., Nix, W., Hwang, K., Gao, H. (2001). Effect of intrinsic lattice resistance in strain gradient plasticity. *Acta Materialia*, 49(19), 3949–3958.

Rabinowicz, E. (1965). *Friction and Wear of Materials*. John Wiley & Sons, New York.

Ranjith, K. and Rice, J. (2001). Slip dynamics at an interface between dissimilar materials. *Journal of the Mechanics and Physics of Solids*, 49(2), 341–361.

Ren, N. and Lee, S.C. (1994). The effects of surface roughness and topography on the contact behavior of elastic bodies. *Journal of Tribology*, 116(4), 804–810.

Renard, Y. (1998). Modélisation des instabilités liées au frottement sec des solides élastiques, aspects théoriques et numériques. PhD Thesis, LMC-IMAG Grenoble, Grenoble.

Renard, F., Candela, T., Bouchaud, E. (2013). Constant dimensionality of fault roughness from the scale of micro-fractures to the scale of continents. *Geophysical Research Letters*, 40(1), 83–87.

Renardy, M. (1992). Ill-posedness at the boundary for elastic solids sliding under Coulomb friction. *Journal of Elasticity*, 27(3), 281–287.

Rey, V., Anciaux, G., Molinari, J.-F. (2017). Normal adhesive contact on rough surfaces: Efficient algorithm for FFT-based BEM resolution. *Computational Mechanics*, 60(1), 69–81.

Rey, V., Krumscheid, S., Nobile, F. (2019). Quantifying uncertainties in contact mechanics of rough surfaces using the multilevel monte carlo method. *International Journal of Engineering Science*, 138, 50–64.

Rice, J.R. (2006). Heating and weakening of faults during earthquake slip. *Journal of Geophysical Research: Solid Earth*, 111, B05311.

Rice, J.R. and Tse, S.T. (1986). Dynamic motion of a single degree of freedom system following a rate and state dependent friction law. *Journal of Geophysical Research: Solid Earth*, 91(B1), 521–530.

Russ, J.C. (1994). *Fractal Surfaces*. Springer, New York.

Sabnis, P.A., Forest, S., Arakere, N.K., Yastrebov, V.A. (2013). Crystal plasticity analysis of cylindrical indentation on a Ni-base single crystal superalloy. *International Journal of Plasticity*, 51, 200–217.

Sahlin, F., Larsson, R., Almqvist, A., Lugt, P., Marklund, P. (2010). A mixed lubrication model incorporating measured surface topography. Part 1: Theory of flow factors. *Proceedings of the Institution of Mechanical Engineers, Part J: Journal of Engineering Tribology*, 224(4), 335–351.

Sainsot, P., Leroy, J.M., Villechaise, B. (1990). Paper VI (i) Effect of surface coatings in a rough normally loaded contact. *Tribology Series*, 17, 151–156.

Sang, Y., Dubé, M., Grant, M. (2001). Thermal effects on atomic friction. *Physical Review Letters*, 87(17), 174301.

Sayles, R. (1996). Basic principles of rough surface contact analysis using numerical methods. *Tribology International*, 29(8), 639–650.

Sayles, R. and Thomas, T. (1978). Computer simulation of the contact of rough surfaces. *Wear*, 49(2), 273–296.

Schatzman, M. (1978). A class of nonlinear differential equations of second order in time. *Nonlinear Analysis: Theory, Methods and Applications*, 2(3), 355–373.

Seabra, J. and Berthe, D. (1987). Influence of surface waviness and roughness on the normal pressure distribution in the hertzian contact. *Journal of Tribology*, 109(3), 462–469.

Sewerin, F. and Papadopoulos, P. (2017). An exact penalty approach for the finite element solution of frictionless contact problems. In *Proceedings of the 7th GACM Colloquium on Computational Mechanics*, October 11-13. University of Stuttgart, Stuttgart.

Shi, X. and Polycarpou, A.A. (2005). Measurement and modeling of normal contact stiffness and contact damping at the meso scale. *Journal of Vibration and Acoustics*, 127(1), 52–60.

Shvarts, A.G. (2019). Coupling mechanical frictional contact with interfacial fluid flow at small and large scales. PhD Thesis, PSL Research University, MINES ParisTech, Paris.

Shvarts, A.G. and Yastrebov, V.A. (2018a). Fluid flow across a wavy channel brought in contact. *Tribology International*, 126, 116–126.

Shvarts, A.G. and Yastrebov, V.A. (2018b). Trapped fluid in contact interface. *Journal of the Mechanics and Physics of Solids*, 119, 140–162.

Shyu, S., Chang, T., Saleeb, A. (1989). Friction-contact analysis using a mixed finite element method. *Computers & Structures*, 32(1), 223–242.

Simo, J. and Hughes, T. (1998). *Computational Inelasticity*. Springer, New York.

Simoes, F. and Martins, J. (1998). Instability and ill-posedness in some friction problems. *International Journal of Engineering Science*, 36(11), 1265–1293.

Song, Z. and Komvopoulos, K. (2013). Elastic-plastic spherical indentation: Deformation regimes, evolution of plasticity, and hardening effect. *Mechanics of Materials*, 61, 91–100.

Song, W., Li, L., Ovcharenko, A., Jia, D., Etsion, I., Talke, F.E. (2012). Plastic yield inception of an indented coated flat and comparison with a flattened coated sphere. *Tribology International*, 53, 61–67.

Song, H., Vakis, A., Liu, X., Van der Giessen, E. (2017). Statistical model of rough surface contact accounting for size-dependent plasticity and asperity interaction. *Journal of the Mechanics and Physics of Solids*, 106, 1–14.

Spence, D. (1968). Self similar solutions to adhesive contact problems with incremental loading. *Proceedings of the Royal Society of London. Series A. Mathematical and Physical Sciences*, 305(1480), 55–80.

Spence, D. (1975). The hertz contact problem with finite friction. *Journal of Elasticity*, 5, 297–319.

Spinu, S. and Frunza, G. (2015). The hysteretic behaviour of partial slip elastic contacts undergoing a fretting loop. *Journal of Physics: Conference Series*, 585, 012007.

Stanley, H.M. and Kato, T. (1997). An FFT-based method for rough surface contact. *J. Tribol-T ASME*, 119, 481–485.

Stingl, B., Ciavarella, M., Hoffmann, N. (2013). Frictional dissipation in elastically dissimilar oscillating hertzian contacts. *International Journal of Mechanical Sciences*, 72, 55–62.

Storåkers, B. and Elaguine, D. (2005). Hertz contact at finite friction and arbitrary profiles. *Journal of the Mechanics and Physics of Solids*, 53(6), 1422–1447.

Straffelini, G. (2001). A simplified approach to the adhesive theory of friction. *Wear*, 249(1/2), 78–84.

Stupkiewicz, S., Lengiewicz, J., Sadowski, P., Kucharski, S. (2016). Finite deformation effects in soft elastohydrodynamic lubrication problems. *Tribology International*, 93, 511–522.

Sun, L. (2012). Étude numérique de l'amorçage et de la propagation de fissures de fretting. PhD Thesis, MINES ParisTech, Paris.

Sun, Y., Bloyce, A., Bell, T. (1995). Finite element analysis of plastic deformation of various tin coating/substrate systems under normal contact with a rigid sphere. *Thin Solid Films*, 271(1/2), 122–131.

Svetlizky, I. and Fineberg, J. (2014). Classical shear cracks drive the onset of dry frictional motion. *Nature*, 509(7499), 205.

Svetlizky, I., Muñoz, D.P., Radiguet, M., Kammer, D.S., Molinari, J.-F., Fineberg, J. (2016). Properties of the shear stress peak radiated ahead of rapidly accelerating rupture fronts that mediate frictional slip. *Proceedings of the National Academy of Sciences*, 113(3), 542–547.

Swadener, J., George, E., Pharr, G. (2002). The correlation of the indentation size effect measured with indenters of various shapes. *Journal of the Mechanics and Physics of Solids*, 50(4), 681–694.

Tabor, D. (1951). *The Hardness of Metals*. Oxford University Press, Oxford.

Tan, D. (2003). Mesh matching and contact patch test. *Computational Mechanics*, 31(1/2), 135–152.

Tangena, A. and Wijnhoven, P. (1985). Finite element calculations on the influence of surface roughness on friction. *Wear*, 103(4), 345–354.

Taylor, R. and Papadopoulos, O. (1991). On a patch test for contact problems in two dimensions. In *Nonlinear Computational Mechanics*, Wriggers, P. and Wagner, W. (eds). Springer, Berlin.

Temizer, I. and Stupkiewicz, S. (2016). Formulation of the Reynolds equation on a time-dependent lubrication surface. *Proceedings of the Royal Society A: Mathematical, Physical and Engineering Sciences*, 472(2187), 20160032.

Temizer, I., Wriggers, P., Hughes, T. (2011). Contact treatment in isogeometric analysis with NURBS. *Computer Methods in Applied Mechanics and Engineering*, 200(9/12), 1100–1112.

Temizer, I., Wriggers, P., Hughes, T. (2012). Three-dimensional mortar-based frictional contact treatment in isogeometric analysis with NURBS. *Computer Methods in Applied Mechanics and Engineering*, 209, 115–128.

Thomas, T.R. (1999). *Rough Surfaces*. World Scientific Publishing Co., Singapore.

Thompson, M.K. and Thompson, J.M. (2010). Considerations for the incorporation of measured surfaces in finite element models. *Scanning*, 32(4), 183–198.

Tkalich, D., Yastrebov, V.A., Cailletaud, G., Kane, A. (2017). Multiscale modeling of cemented tungsten carbide in hard rock drilling. *International Journal of Solids and Structures*, 128, 282–295.

Torstenfelt, B.R. (1984). An automatic incrementation technique for contact problems with friction. *Computers & Structures*, 19(3), 393–400.

Vakis, A.I., Yastrebov, V.A., Scheibert, J., Nicola, L., Dini, D., Minfray, C., Almqvist, A., Paggi, M., Lee, S., Limbert, G. et al. (2018). Modeling and simulation in tribology across scales: An overview. *Tribology International*, 125, 169–199.

Venner, C.H. and Lubrecht, A. (1996). Numerical analysis of the influence of waviness on the film thickness of a circular EHL contact. *Journal of Tribology*, 118(1), 153–161.

Vlădescu, S.-C., Putignano, C., Marx, N., Keppens, T., Reddyhoff, T., Dini, D. (2019). The percolation of liquid through a compliant seal – An experimental and theoretical study. *Journal of Fluids Engineering*, 141(3), 031101.

Webster, M. and Sayles, R. (1986). A numerical model for the elastic frictionless contact of real rough surfaces. *Journal of Tribology*, 108(3), 314–320.

Wei, Z., Li, Z., Qian, Z., Chen, R., Dollevoet, R. (2016). 3D FE modelling and validation of frictional contact with partial slip in compression-shift-rolling evolution. *International Journal of Rail Transportation*, 4(1), 20–36.

West, M. and Sayles, R. (1987). A 3-dimensional method of studying 3-body contact geometry and stress on real rough surfaces. *Tribology Series*, 12, 195–200. doi: 10.1016/S0167-8922(08)71066-6.

Whitehouse, D.J. (2010). *Handbook of Surface and Nanometrology*. CRC Press, Boca Raton.

Willis, J. (1966). Hertzian contact of anisotropic bodies. *Journal of the Mechanics and Physics of Solids*, 14(3), 163–176.

Willis, J. (1967). Boussinesq problems for an anisotropic half-space. *Journal of the Mechanics and Physics of Solids*, 15(5), 331–339.

Wilson, W. and Sheu, S. (1988). Real area of contact and boundary friction in metal forming. *International Journal of Mechanical Sciences*, 30(7), 475–489.

Wriggers, P. (2006). *Computational Contact Mechanics*, 2nd edition. Springer, Berlin, Heidelberg.

Wriggers, P. (2008). *Nonlinear Finite Element Methods*. Springer, Berlin, Heidelberg.

Wriggers, P. and Krstulović-Opara, L. (2000). On smooth finite element discretizations for frictional contact problems. *ZAMM-Journal of Applied Mathematics and Mechanics/Zeitschrift für Angewandte Mathematik und Mechanik*, 80(S1), 77–80.

Wriggers, P. and Zavarise, G. (1993). Application of augmented Lagrangian techniques for non-linear constitutive laws in contact interfaces. *Communications in Numerical Methods in Engineering*, 9(10), 815–824.

Wriggers, P. and Zavarise, G. (2008). A formulation for frictionless contact problems using a weak form introduced by Nitsche. *Computational Mechanics*, 41(3), 407–420.

Wriggers, P., Krstulović-Opara, L., Korelc, J. (2001). Smooth C1-interpolations for two-dimensional frictional contact problems. *International Journal for Numerical Methods in Engineering*, 51, 1469–1495.

Yang, B., Laursen, T., Meng, X. (2005). Two dimensional mortar contact methods for large deformation frictional sliding. *International Journal for Numerical Methods in Engineering*, 62, 1183–1225.

Yastrebov, V.A. (2013). *Numerical Methods in Contact Mechanics*. ISTE Ltd, London, and John Wiley & Sons, New York.

Yastrebov, V.A. (2016). Sliding without slipping under coulomb friction: Opening waves and inversion of frictional force. *Tribology Letters*, 62(1), 1–8.

Yastrebov, V.A. (2019). The elastic contact of rough spheres investigated using a deterministic multi-asperity model. *Journal of Multiscale Modelling*, 10(1), 1841002.

Yastrebov, V.A., Durand, J., Proudhon, H., Cailletaud, G. (2011). Rough surface contact analysis by means of the finite element method and of a new reduced model. *Comptes Rendus Mécanique*, 339(7/8), 473–490.

Yastrebov, V.A., Anciaux, G., Molinari, J.-F. (2014). The contact of elastic regular wavy surfaces revisited. *Tribology Letters*, 56(1), 171–183.

Yastrebov, V.A., Anciaux, G., Molinari, J.-F. (2015). From infinitesimal to full contact between rough surfaces: Evolution of the contact area. *International Journal of Solids and Structures*, 52, 83–102.

Yastrebov, V.A., Anciaux, G., Molinari, J.-F. (2017a). On the accurate computation of the true contact-area in mechanical contact of random rough surfaces. *Tribology International*, 114, 161–171.

Yastrebov, V.A., Anciaux, G., Molinari, J.-F. (2017b). The role of the roughness spectral breadth in elastic contact of rough surfaces. *Journal of the Mechanics and Physics of Solids*, 107, 469–493.

Yoon, E.-S., Singh, R.A., Kong, H., Kim, B., Kim, D.-H., Jeong, H.E., Suh, K.Y. (2006). Tribological properties of bio-mimetic nano-patterned polymeric surfaces on silicon wafer. *Tribology Letters*, 21(1), 31–37.

Zahouani, H., Vargiolu, R., Loubet, J.-L. (1998). Fractal models of surface topography and contact mechanics. *Mathematical and Computer Modelling*, 28(4/8), 517–534.

Zavarise, G. and De Lorenzis, L. (2009a). A modified node-to-segment algorithm passing the contact patch test. *International Journal for Numerical Methods in Engineering*, 79(4), 379–416.

Zavarise, G. and De Lorenzis, L. (2009b). The node-to-segment algorithm for 2D frictionless contact: Classical formulation and special cases. *Computer Methods in Applied Mechanics and Engineering*, 198(41/44), 3428–3451.

Zavarise, G., Wriggers, P., Stein, E., Schrefler, B.A. (1992). Real contact mechanisms and finite element formulation – A coupled thermomechanical approach. *International Journal for Numerical Methods in Engineering*, 35(4), 767–785.

Zhang, H., Wang, H., Wriggers, P., Schrefler, B. (2005). A finite element model for contact analysis of multiple cosserat bodies. *Computational Mechanics*, 36(6), 444–458.

Zienkiewicz, O. and Taylor, R. (2000a). *The Finite Element Method, Volume 1: The Basis*, 5th edition. Butterworth-Heinemann, Oxford.

Zienkiewicz, O. and Taylor, R. (2000b). *The Finite Element Method, Volume 2: Solid Mechanics*, 5th edition. Butterworth-Heinemann, Oxford.

Zisis, T., Gourgiotis, P., Baxevanakis, K.P., Georgiadis, H. (2014). Some basic contact problems in couple stress elasticity. *International Journal of Solids and Structures*, 51(11/12), 2084–2095.